Author's response

Part 1
Response to Dr. David Webb by Guohong Fang and Di Wu

Overview

This is a classic semi-analytical study of a partially enclosed tidal system. The mathematics is fairly straightforward but the authors use the results to obtain a better physical understanding for the position of the amphidromes in the strait between Korea and Japan. The paper is well laid out and easy to read and understand. I think that in principal it should be published.

Reply: We sincerely thank Dr.Webb for his careful reading of our manuscript and constructive comments and suggestions, which are of great help in improving our study. We have addressed all these comments; our responses are given below.

Main suggestions

As I said the mathematics is fairly straightforward (maybe that is why JPO rejected the m/s), so I do not think all the details are needed in the final paper. In particular I think that the content of the appendices may be better placed in a separate document as supplementary material (a possibility with Ocean Science).

Reply: The appendix has been deleted and will be submitted separately in the form of supplementary material.

I am also concerned that this branch of oceanic literature always ignores similar studies that have occurred in related fields of physics - in particular microwave wave guides. There used to be a complaint about the different branches of physics reinventing the wheel and to a certain extent this is true here as the Coriolis term does not necessarily introduce major changes.

For that reason I suggest that the authors, who appear to be applied mathematicians, talk to someone with a physics or microwave background about reflections from discontinuities in impedance (refractive index in the case of light). This should give a bit more insight which they could usefully add to their conclusions.

Reply: The behaviour of water wave reflection in a nonrotating channel is indeed similar to the microwave reflection, or the light refraction. However, when the wave propagates in a rotating channel and the period of the wave is comparable to that of Earth's rotation the Coriolis force will have significant influence on the wave propagation and reflection. As an example, we revisit the problem of the reflection of the Kelvin wave in a semi-infinite channel first studied by Taylor (1922). Taylor' result shows that when the incident Kelvin wave is reflected at the southern shore of the North Sea, a time lag of 1.4 hr occurs due to the Coriolis force. The details are given in the appendix to this response. The main conclusion is that the Coriolis parameter has significant influence on the tidal wave reflection in a semi-infinite channel. This conclusion should also hold for the case studied in the present paper.

As another possibility for future work I would also suggest treating all variables as complex and investigating how the solutions at key points change with complex angular velocity - to understand how the resonant properties of the system affect the solution.

Reply: This is a very useful suggestion for our future work. We will try to apply the complex angular velocity to the Taylor method.

Detailed comments

1. Title

I suggest "Study of the ..."

Reply: Revised as suggested.

2. Page 1, line 9

Similarly "studies of the tides ..."

Reply: Revised as suggested.

3. Page 1, line 23

" ... the Yellow Sea ..."

Reply: Revised as suggested.

4. Page 1, line 26

Delete ’vast’.

Reply: Revised as suggested.

5. Page 1, line 27

Knives are sharp, continental slopes are steep.

Reply: The word “sharp” has been replaced with “steep” in page 1, line 27 and page 16, line 4.

6. Page 2, line 18

I disagree with ’analytical’, this is a semi-analytical method, using the numerical solution of a large set of equations.

Reply: The word “analytical” has been replaced with “semi-analytical”.

7. Page 4, line 21

This is angular velocity (radians per second) Anything with frequency refers to full cycles of something.

Reply: The term “angular frequency” has been replaced with “angular velocity” in page 1, line 18, page

4, line 21 and page 5, line 13. (Please note that angular frequency is a synonym of angular velocity, see Weik M.H. (2000) angular frequency. In: Computer Science and Communications Dictionary. Springer, Boston, MA. https://doi.org/10.1007/1-4020-0613-6_670).

8. Page 5, line 8
Change to 'with momentum ... "

Reply: The article "the" has been deleted.

9. Page 16, lines 10 onwards.
This is all very standard in other areas of physics as well, so I do not think the work of Dean and Dalrymple needs to be spelt out in such detail. I suggest that you just give the results you need.

Reply: According to this comment, we have revised this paragraph as follows: "If the second area is semi-infinitely long, allowing for the wave to radiate out from the second area freely, then a part of the wave is reflected at the connecting point and another part is transmitted into the second area. The amplitude of the transmitted wave is (see e. g. Dean and Dalrymple (1984))"

10. Page 17, line 1
You do not make clear which case you are writing about - yours or that of Dean and Dalrymple.

Reply: This equation is the same as that given by Dean and Dalrymple (1984), but in a more understandable form. In order to clarify this the words "(see also Dean and Dalrymple (1984))" have been added above this equation.

11. Page 18, line 9 and following
"can be attributed to ...". This is a bit of a cop out, the classic response of a committee shirking responsibility. It would read better if you were disappointed about the discrepancy but that it may be due to ... .

Reply: The words "can be attributed to" have been replaced with "may be duo to".

12. Page 19, Line 21.
I would suggest you delete this line. It is doing nothing useful.

Reply: This line has been deleted.

Appendix: A Short Note on the Reflection of the Kelvin Wave in a Semi-infinite Channel: Taylor's Example Revited

1. Introduction

Taylor (1922) studied the tidal system in a semi-infinite channel, with especial attention paid to the refection of the Kelvin wave at the closed end of the channel. The channel he studied is semi-infinite with a width of W and a uniforn depth of h as shown in Fig. 1. He showed that when an incident

Kelvin wave propagates into the rotating channel, the wave would be reflected at the closed end to form a reflected Kelvin wave and an amphidromic system. Meanwhile, a series of Poincare modes would be induced in the vicinity of the closed end.

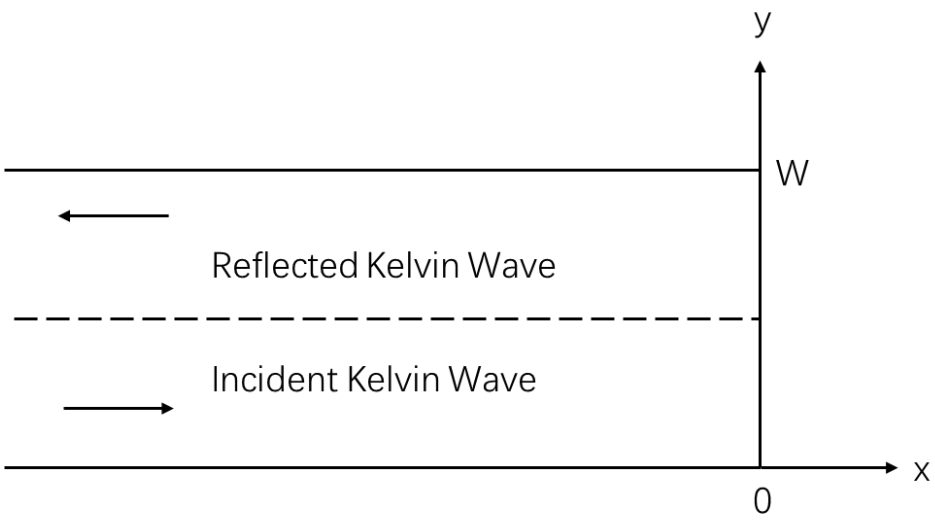

Fig.A1 Sketch of the semi-infinite channel.

2. Taylor's Example

Let

$$\begin{cases} \alpha = \frac{f}{c}, \\ k = \frac{\sqrt{\sigma^2+f^2}}{c}, \end{cases} \tag{R1}$$

where f is Coriolis parameter, σ is the angular velocity of the wave, c is defined as

$$c = \frac{\pi}{W}\sqrt{gh} \tag{R2}$$

with W and h representing the width and depth of the channel respectively. Taylor (1922) specifically computed the relationship between the incident and reflected Kelvin waves with period equal to 12 hr (equivalent to an angular velocity of $1.4544 \times 10^{-4}\mathrm{s}^{-1}$) for the case

$$\begin{cases} \alpha = 0.7, \\ k = 0.5, \end{cases} \tag{R3}$$

which corresponds to the dimensions of the North Sea. This case was referred to as Taylor's example by Brown (1973). The estimated phase-lag increase θ of the reflected Kelvin wave versus the incident Kelvin wave at the closed end of the channel was equal to 42.10° (Taylor, 1920, p. 166). This result indicates that when the incident Kelvin wave is reflected at the southern shore of the North Sea, a time lag of 1.4 hr occurs due to the Coriolis force. The value of θ was estimated again by Brown (1973), yielding θ =42.18° (see also Thiebaux, 1988, p.369).

3. Influence of the Coriolis parameter on the reflection of the incident Kelvin wave

To illustrate the Influence of the Coriolis parameter on the reflection of the incident Kelvin wave, we artificially change the values of the Corisolis parameter, and apply the method discribed in our paper to the semi-infinite channel shown in Fig.1. The channel is taken 463.3 km wide (corresponding to 250 nautical miles as given by Taylor (1922)) and 63.4 m deep, then we truncate the Poincare modes up to 100 terms and calculate the values of θ for various values of f. The result is shown with the red curve

in Fig. 2. This figure indicates that the value of θ is zero when $f = 0$, and can be up to nearly 50° when $f = 1.4 \times 10^{-4}\mathrm{s}^{-1}$.

For the case of Tayor's example which satisfies Eq. (3) we can obtain $f = 1.1835 \times 10^{-4}\mathrm{s}^{-1}$ through eliminating c in Eq. (1) and inserting Eq. (3). This particular value of f is indicated with a vertical dashed line in Fig.2, and the corresponding value of θ is 42.16°.

Fang and Wang (1966) proposed an approximate equation for θ as follows (note that the Eq. (60) of their paper is the expression for $\theta/2$):

$$\theta = \frac{8\nu^3}{\pi l(l^2+\nu^2)\sqrt{l^2+\nu^2-1}\,\mathrm{th}\frac{\pi\nu}{2l}}, \tag{R4}$$

where

$$\nu = \frac{f}{\sigma}, \tag{R5}$$

and

$$l = \frac{c}{\sigma}. \tag{R6}$$

The values of θ derived from (4) as function of f are shown in blue curve in Fig. 2. In particular, the value of θ corresponding to $f = 1.1835 \times 10^{-4}\mathrm{s}^{-1}$ is equal to 41.68°.

Thiebaux (1988) also proposed an approximate method for calculating θ. His equation has the form

$$\theta = b_1\nu' + b_3\nu'^3 + O(\nu'^5) \tag{R7}$$

where

$$\nu' = \frac{\sigma}{f}. \tag{R8}$$

Thiebaux (1988) did not provide any formula for calculating $O(\nu'^5)$. The expressions of b_1 and b_3 are quite complicated, but their values can be calculated from his Eqs. (30) and (31) and his Table 1. The values of θ derived from (7) as function of f are shown in green curve in Fig. 2. In particular, the value of θ corresponding to $f = 1.1835 \times 10^{-4}\mathrm{s}^{-1}$ is equal to 37.19°.

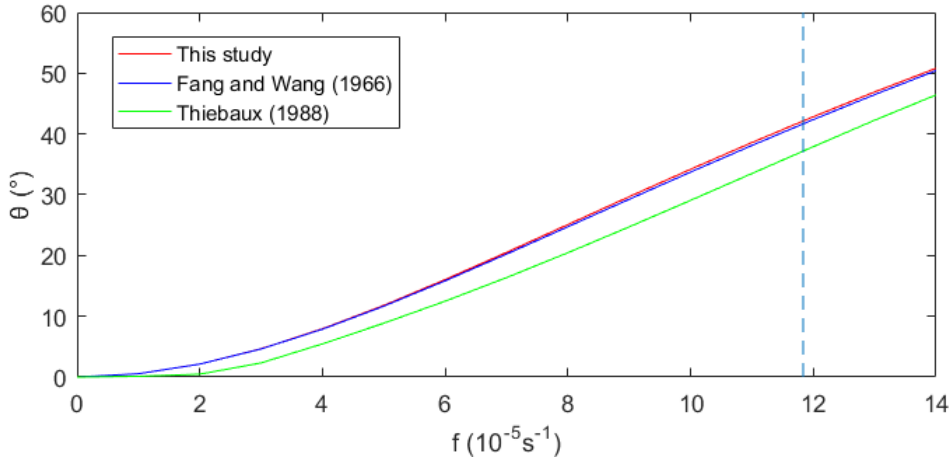

Fig. 2 The phase-lag increase (θ) of the reflected Kelvin wave versus the incident Kelvin wave at the closed end as function of the Coriolis parameter (f) in a semi-infinite channel, which has a width of 463.3 km and a unifom depth of 63.4 m.

4. Conclusion

The works of Taylor (1922), Fang and Wang (1966), Brown (1973), Thiebaux (1988) and the present study all show that the Coriolis parameter has significant influence on the tidal wave reflection in a semi-infinite channel.

References

Brown, P. J.: Kelvin-wave reflection in a semi-infinite canal. J. Mar. Res., 31, 1-10, 1973.

Fang, G., and Wang, J.: Tides and tidal streams in gulfs, Oceanol. Limnol. Sin., 8, 60–77, 1966. (in Chinese with English abstract).

Taylor, G. I.: Tidal oscillations in gulfs and rectangular basins. Proc. London Math. Soc., Ser. 2, 20, 148-181, https://doi.org/10.1112/plms/s2-20.1.148, 1922.

Thiebaux, M. L.: Low-frequency Kelvin wave reflection coefficient. J. Phys. Oceanogr., 18, 367-372, https://doi.org/10.1175/1520-0485(1988)018<0367:LFKWRC>2.0.CO;2, 1988.

Part 2
Response to Referee #2 by Guohong Fang and Di Wu

This paper contains an original contribution to the co-oscillating tide in Sea of Japan (East Sea) using an extended Taylor method. Writing is considered to be reasonably good with fine piece of references. However, there is an important point authors need to make correction to enhance the quality of the paper. Specifically, extension of the three sub-region model to four sub-region model is requested. Reviewer think the extension work is not difficult but considerable time around two months might be required to make correction of the content of manuscript. For that, a major revision is recommended.

Reply: We sincerely thank Reviewer for his carefully reading and constructive comments. We have extended the model domain from three sub-regions to four sub-regions in the revised manuscript. Please see the following for details.

Detailed comments:

Pg.4, Lines 14-20: Authors constructed a model with three sub-regions as seen in Fig. 3. However, water depth of Fig.1 and tidal chart of Fig.2 indicate the necessity of including Tartar Strait region in the analytical model. Extension of the three sub-region model to the four sub-region model is requested. On the while, review think, though not much important, representing the Japan Sea (East Sea) as the Area 2 with width W1+W3 might be sufficient rather than width W2 unless the shallow water depth along the northern coastline of Japan is considered.

Reply: According to this comment, we have extended the model domain from three sub-regions to four sub-regions in the revised manuscript. For convenience, we call the models with three sub-regions and with four sub-regions the 3-area model and the 4-area model respectively. The 4-area model domain fitting the KS and JS is shown in Fig. R1 below. Please note that we can only artificially place Area4 northeast of Area3 rather than north of Area3 due to the limitation of the Taylor method. So that the Area4 cannot overlap the actual Tartar Strait.

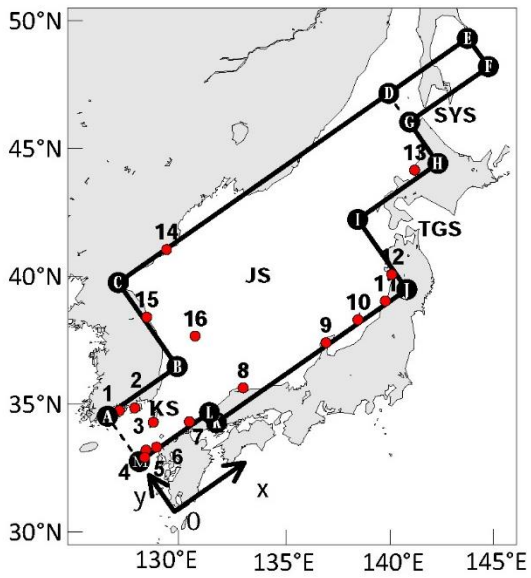

Fig. R1: Idealized 4-area model domain fitting the Korea Strait and Japan Sea. Copied from Figure 4 of the revised manuscript.

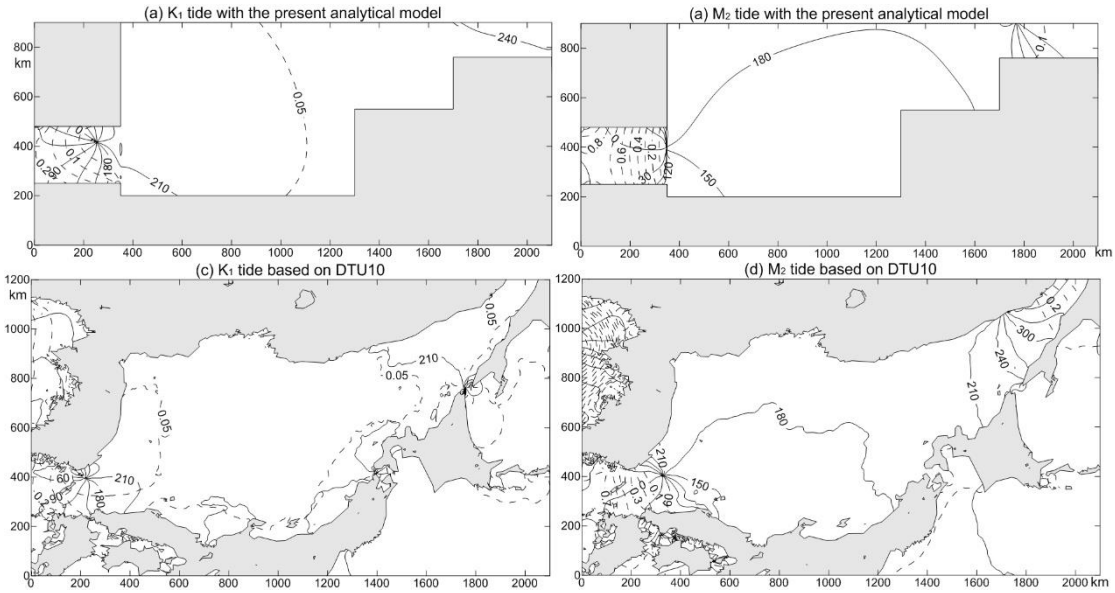

Fig. R2: Comparison of tidal system charts. (a) K_1 and (b) M_2 tides from the present analytical model; and (c) K_1 and (d) M_2 tides from DTU10 (Chen and Andersen, 2011). Copied from Figure 5 of the revised manuscript.

The comparison between model results and observations is shown in Fig. R2. Correspondingly, the results in Area1 (representing the KS) of the 3-area model mentioned from page 13, line 29 to page 14, line 14 in the original manuscript are replaced with the 4-area model results in the revised manuscript. The changes in Area1 are less than 0.01 m and 2° for amplitudes and phase lags of K_1 respectively, and less than 0.01 m and 1° for amplitudes and phase lags of M_2 respectively, indicating that adding Area4 does not significantly change the tidal systems in Area1.

Pg.7, Line 16: Authors used the Collocation approach. In fact there is another approach called Galerkin approach. Briefly comment why authors used Collocation approach. Is it mainly due to its simplicity?

Reply: Yes, it is mainly due to its simplicity. In Taylor's original work, he used the Fourier method, which involved the Fourier expansions at the closed cross-sections, and thus making the solution more complicated. To our knowledge, nobody has employed the Galerkin method in the Taylor problem, though it has been widely used in the numerical computations.

Pg.8, Lines 11-12: Authors state that the influence of tide-generating force on the KS is negligible. Reviewer does not agree on this statement because the influence of direct tide generating force (DTGF) on the tide in JS can be significantly large, indirectly affecting on the tide in KS even though its direct influence on the KS is small. Reviewer think co-oscillating tide may be dominant in Japan Sea (East Sea) but DTGF has some non-negligible effects.

Reply: This comment correctly points out a limitation of the Taylor method. The classical and extended Taylor methods solve the homogeneous differential equations as shown in the governing equations in

our manuscript (please see also Taylor, 1922; Hendershott and Speranza, 1971; among others). Once the DTGF is included, the governing equations will become non-homogeneous, and the basic wave forms (namely the Kelvin wave and the Poincare wave) will no longer satisfy the governing equations. This is the reason why all existing studies (please see references listed in our manuscript) do not include DTGF.

To examine the influence of the DTGF on the tides in the Korea Strait, we have numerically computed the tides in the Korea Strait and Japan/East Sea with and without DTGF using MIKE21 model, and make comparison between these two results. As an example, Fig. R3 displays the comparison of the model-produced M_2 tidal systems with and without DTGF.

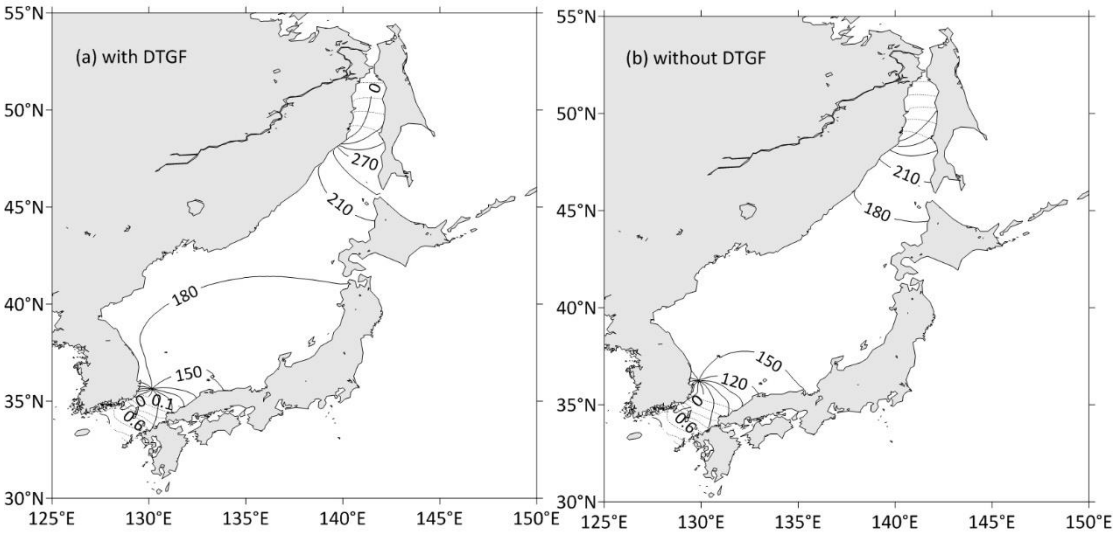

Fig. R3: Comparison of the model-produced M_2 tidal system charts, (a) with DTGF, and (b) without DTGF.

As shown in our paper title, the present study focuses on the tides in the KS. To quantitatively evaluate the influence of the DTGF on the tides in the KS, we select evenly distributed 893 points in the KS as shown in Fig. R4, and calculate the root-mean-square (RMS) vector differences between two sets of model results according the following equation:

$$\Delta = \left\{\frac{1}{K}\sum_{k=1}^{K}\left[\left(H_{2,k}\cos G_{2,k} - H_{1,k}\cos G_{1,k}\right)^2 + \left(H_{2,k}\sin G_{2,k} - H_{1,k}\sin G_{1,k}\right)^2\right]\right\}^{1/2} \quad \text{(R1)}$$

in which $k = 1, 2, \ldots, K$ are indices of the points shown in Fig. R4, with K representing the total number of the points (=893); H and G are model-produced amplitude and phase lag respectively, with subscripts 1 and 2 representing the results with and without DTGF respectively. The characteristic model-produced mean amplitude with DTGF can be calculated from the following equation:

$$\bar{H} = \left(\frac{1}{K}\sum_{k=1}^{K} H_{1,k}^2\right)^{1/2} \quad \text{(R2)}$$

The relative difference is represented by

$$\delta = \Delta/\bar{H} \quad \text{(R3)}$$

The results are given in Table R1 below. From Table R1 we find that the differences between the model results in the KS with and without DTGF are not significant, indicating that the KS is dominated by co-oscillating tides.

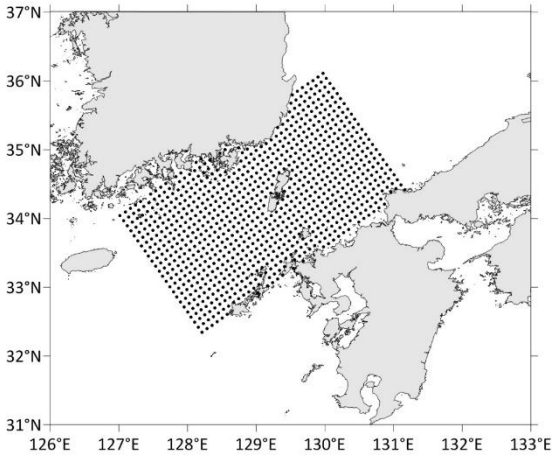

Fig. R4: Distribution of the points for comparison between the model-produced results with and without DTGF.

Table R1. Difference and relative difference between model results with and without direct tidal generating force (DTGF)

	Δ	$\bar{H}$	δ
M2	0.0092	0.6731	0.0137
K1	0.0075	0.1625	0.0459

Pg.9, Lines 10-12: In Table 1, it is noted that water depth of area 3 is 1783m, which is comparable with that of Area 2. With the model reproduction of tide in Tartar Strait shown in Fig.2 is hardly expected.

Reply: We have changed Table 1 to include Area4, which represents the Tartar Strait. The depth of Area4 is taken 90 m, much shallower than Area3.

Pg.11, Lines 11-12: Authors' statement such that the model-produced tidal systems agree fairly well with the DTU10 result is reasonably acceptable. Reviewer however notices that there are some important points authors did not comment. Close examination of Fig.5 reveals that DTU10 produces amphidromic point further north than that calculated by the analytic model and that DTU10 and analytic model produces different contour patterns in Area 2 and Area 3. Reviewer thinks that these are due to neglecting the shallow Tartar Strait region in the analytic model. Again it is addressed that Area 3 is too deep and short to include the effects of presence of the Tartar Strait. According to reviewer's modeling experience, the tides in JS (East Sea) and KS vary sensitively with change of bottom frictional coefficient in the Tartar Strait.

Reply: We accept this comment and add the fourth sub-region (Area4) to represent the Tartar Strait in the revised manuscript. The water depth of Area4 is taken 90 m, which is equal to the mean depth of the main part of the Tartar Strait. After adding Area4, the agreement between model results and DTU10 data is slightly improved.

Pg.12, Lines 3-5: Authors state with regard to Fig. 6 that the greatest phase lag error occurred at the northernmost corner of JS due to the existence of degenerated amphidromic point near the area. This

supports the necessity of developing an extended model which takes into account the shallow Tartar Strait region.

Reply: The 4-area model does show a degenerated amphidromic point for M_2 in Area4, which is consistent with observed feature as shown in Fig. R2.

Pg.16, Line 1: Authors discussed tidal dynamics in KS-JS basin with emphasis on the amphidromic point. However, it is hard to find any discussions related to the influence of Area 2. Reviewer think this is because no meaningful contribution by Area 2. Again, it is strongly addressed that extension of the three sub-region model to the four subregion model is required.

Reply: In the text of the original manuscript from page 17, line 6 onward in Section 4 our focus of discussion is on the role of Area2 which representing the JS. To emphasize the importance of the JS, we insert "Eq. (36) indicates that the length, width and depth of Area2 are also important in determining the phase-lag increase of the reflected wave relative to the incident wave in Area1" in page 17 of the revised text; and add "(5) The length, width and depth of the JS is also important in determining the phase-lag increase of the reflected Kelvin wave in the KS" to the end of Section 5 (Summary) in the revised text.

Part 3

Modification list

Page 1.

Line 1. The title “Study on ”has been changed to “Study of …”.

Line 9. “studies on” has been changed to “studies of”.

Line 10. “…three connected uniform-depth rectangular areas…” has been changed to “…four connected uniform-depth rectangular areas…”.

Line 18. “angular frequency” has been changed to “angular velocity”.

Line 23. The word “the” has been added before “Yellow Sea”.

Line 26. The word “vast” has been deleted.

Line 27. “A sharp continental” has been changed to “A sheep continental”.

Page 2.

Line 18. “analytical solutions” has been changed to “semi-analytical solutions”.

Page 3.

Line1. Figure 1 has been replaced by a new figure with “TTS”, and “TTS-Tartar Strait” has been added in the caption.

Page 4.

Lines 2-3. “an analytical solution” has been changed to “a theoretical solution”.

Line 18. Figure 3 has been replaced by a new figure with a four-rectangle structure.

Line 21. “angular frequency” has been changed to “angular velocity”.

Page 5.

Line 8. The word “the” before “momentum advection” has been deleted.

Line 13. “angular frequency” has been changed to “angular velocity”.

Page 6.

Line 23. “both the idealized KS and JS” has been changed to “all rectangular areas shown in Fig.3”.

Page 8.

Line 17. “three rectangular areas” has been changed to “four rectangular areas”.

Line 18. “our area of focus” has been changed to “our focus area”.

Line 19. “two rectangles” has been changed to “three rectangles”.

Line 22. “angular frequencies” has been changed to “angular velocities”.

Page 9.

Lines 1-3. Figure 4 has been replaced by a new figure with a four -rectangle structure, and “A, B, … , J” in the caption has been changed to “A, B,…, M”.

Lines 5-6. “… in these three areas are 2686 km, 12189 km, and 11398 km, respectively, and those of the M_2 Kelvin waves are 1393 km, 6321 km, and 5911 km, respectively” has been changed to “… in these

four areas are 2686 km, 12189 km, 11398 km, and 2561 km, respectively, and those of the M_2 Kelvin waves are 1393 km, 6321 km, 5911 km and 1328 km, respectively."
Lines 12. The fifth column about Area4 has been inserted in Table 1.

Page 11.
Lines 1-2. Figure 5 has been replaced by a new figure with new solutions, and "analytical model" in the caption has been changed to "theoretical model".
Lines 4-6. Figure 6 has been replaced by a new figure with new solutions, and "A, B, … , J" in the caption has been changed to "A, B, C, D, G, H, I, J K, L, M".
Line 11. The sentence "A degenerated amphidromic point appears near the entrance of the Tartar Strait." has been inserted.

Page 12.
Line 4. "approximately 70° at the northernmost corner of the JS" has been changed to "approximately 64° near the entrance of the Tartar Strait".
Line 9. The RMS differences "0.014 and 0.031 m" and "7.4° and 6.4° have been changed to "0.014 and 0.032 m" and "7.0° and 5.2°", respectively.
Line 12. Table 3 has been replaced with the new solutions.

Page 13.
Line18. "0.96 cm" has been changed to "0.95 cm".

Page 13 Line 30 ~Page 14 Line 14.
All the data have been replaced with the new solutions, which is shown as follows:

"The incident and reflected K_1 Kelvin waves are shown in Figs. 7c and 7d, respectively. The area-mean amplitude of the incident Kelvin wave in the KS is 0.248 m, and that of the reflected Kelvin wave is 0.190 m, which is 77% of the incident Kelvin wave. On the connecting cross-section, the section-mean amplitude of the incident Kelvin wave is 0.243 m, and the section-mean phase lag is 151.6°. The section-mean amplitude of the reflected Kelvin wave is 0.194 m, which is 80% of the incident Kelvin wave. The section-mean phase lag is 295.8°, indicating that the phase lag increases by 144.2° when the wave is reflected. The amphidromic point of the superposed Kelvin wave is 137 km away from the step and close to the northwest shore of the KS.

The incident and reflected M_2 Kelvin waves are shown in Figs. 8c and 8d, respectively. The area-mean amplitude of the incident Kelvin wave in the KS is 0.471 m, and that of the reflected Kelvin wave is 0.439 m, which is 93% of the incident Kelvin wave. This ratio is larger than the K_1 tide because the bottom friction of M_2 is smaller and less energy is lost in the propagation process. On the connecting cross-section, the mean amplitude of the incident Kelvin wave is 0.462 m, and the phase lag is 97.9°. The mean amplitude of the reflected Kelvin wave is 0.447 m, which is 97% of the incident Kelvin wave, and the phase lag is approximately 266.4°, with a phase-lag increase of 168.5°, which is closer to 180° as compared to the corresponding value of the K_1 tide. Accordingly, the M_2 amphidromic point of the superposed Kelvin wave shifts to approximately 21 km away from the step. A comparison between Fig. 7a and Fig. 8a shows that the amphidromic point of K_1 is located west of that of M_2. This result reproduces well the observed phenomenon as seen from Fig. 2."

Page 15.

Lines 1-4 Figure 7 and figure 8 have been replaced with the new solutions.

Page 16.

Lines 4-5. “a sharp continental slope” has been changed to “a steep continental slope”.

Lines 10-14. “Dean and Dalrymple (1984) have presented a solution for a tidal waves travelling in such a channel; however, in their study, 10 the wave was allowed to radiate out from the second area freely, which implies that the second area is assumed to be semi-infinitely long. Their solution shows that a part of the wave is reflected at the connecting point and another part is transmitted into the second area.” has been changed to “If the second area is semi-infinitely long, allowing for the wave radiating out from the second area freely, then a part of the wave is reflected at the connecting point and another part is transmitted into the second area. The amplitude of the transmitted wave is (see e. g. Dean and Dalrymple (1984))”.

Page 17.

Line 1. “Appendix for derivation” has been change to “also Dean and Dalrymple (1984)”.

Line 12. “Appendix” has been changed to “supplement”

Line 16 The sentence “Eq. (36) indicates that the length, width and depth of Area2 are also important in determining the phase-lag increase of the reflected wave relative to the incident wave in Area1.” has been added after “$\chi_2 = k_2 L_2$.”

Page 18.

Line 9. “can be attributed to” has been changed to “may be due to”.

Page 19

Line 20. “(5) The length, width and depth of the JS is also important in determining the phase-lag increase of the reflected Kelvin wave in the KS.” has been added at the end of the paragraph.

Line 21. The last sentence has been deleted.

Pages 20-23

The Appendix has been deleted in the manuscript, and will be submitted as a supplement.

Page 24

Line 15. “We sincerely thank Dr. Joanne Williams for handling our manuscript and thank Dr. David Webb and the anonymous Referee for their careful reading of our manuscript and constructive comments and suggestions which are of great help in improving our work.” has been added in acknowledgment.

Study of the Tidal Dynamics of the Korea Strait Using the Extended Taylor Method

Di Wu[1], **Guohong Fang**[1,2], **Zexun Wei**[1,2], **Xinmei Cui**[1,2]

[1]First Institute of Oceanography, Ministry of Natural Resources, Qingdao, 266061, China
[2]Laboratory for Regional Oceanography and Numerical Modeling, Pilot National Laboratory for Marine Science and Technology, Qingdao, 266237, China

Correspondence: Guohong Fang (fanggh@fio.org.cn)

Abstract. The Korea Strait (KS) is a major navigation passage linking the Japan Sea (JS) to the East China Sea and Yellow Sea. Almost all existing studies of the tides in the KS employed either data analysis or numerical modelling methods; thus, theoretical research is lacking. In this paper, we idealize the KS-JS basin as four connected uniform-depth rectangular areas and establish a theoretical model for the tides in the KS and JS using the extended Taylor method. The model-produced K_1 and M_2 tides are consistent with the satellite altimeter and tidal gauge observations, especially for the locations of the amphidromic points in the KS. The model solution provides the following insights into the tidal dynamics. The tidal system in each area can be decomposed into two oppositely travelling Kelvin waves and two families of Poincaré modes, with Kelvin waves dominating the tidal system. The incident Kelvin wave can be reflected at the connecting cross-section, where abrupt increases in water depth and basin width occur from the KS to JS. At the connecting cross-section, the reflected wave has a phase-lag increase relative to the incident wave by less than 180°, causing the formation of amphidromic points in the KS. The above phase-lag increase depends on the angular velocity of the wave and becomes smaller as the angular velocity decreases. This dependence explains why the K_1 amphidromic point is located farther away from the connecting cross-section in comparison to the M_2 amphidromic point.

1 Introduction

The Korea Strait (KS, also called the Tsushima Strait) connects the East China Sea (ECS) on southwest and the Japan Sea (the JS, also called the East Sea, or the Sea of Japan) on northeast. It is the main route linking the JS to the ECS and the Yellow Sea and is thus an important passage for navigation. The strait is located on the continental shelf, and it has a length of approximately 350 km, a width of 250 km, and an average water depth of approximately 100 m. The JS, which is adjacent to the KS, is a deep basin that has an average depth of approximately 2000 m and a depth of more than 3000 m at its deepest part. A steep continental slope separates the KS and the JS, and it presents abrupt depth and width changes (Fig. 1). Such topographic characteristics create the unique tidal waves that occur in the KS.

Deleted: on
Deleted: on
Deleted: three
Deleted: frequency
Deleted: frequency
Deleted: vast
Deleted: sharp

Ogura (1933) first conducted a comprehensive study of the tides in the seas adjacent to Japan using data from the tidal stations along the coast and gained a preliminary understanding of the characteristics of the tides, including amphidromic systems in the KS. Since then, many researchers have investigated the tides in the strait via observations (Odamaki, 1989a; Matsumoto et al., 2000; Morimoto et al., 2000; Teague et al., 2001; Takikawa et al., 2003) and numerical simulations (Fang and Yang, 1988; Kang et al., 1991; Choi et al., 1999; Book et al., 2004). The results of these studies show consistent structures of the tidal waves in the KS. Fig. 2 displays the distributions of the K_1 and M_2 tidal constituents based on the global tidal model DTU10, which is based on satellite altimeter observations (Cheng and Andersen, 2011). The figures show that the amplitudes of the diurnal tides are smaller than the semidiurnal tides. The peak amplitude of the semidiurnal tide appears on the south coast of South Korea, and lower amplitudes occur along the southern shore of the strait from the ECS to the JS. Distinguishing features include (1) K_1 and M_2 amphidromic points in the strait that appear in the northeast part of the KS close to the southern coast of the Korean Peninsula; and (2) the M_2 amphidromic point appears further northeast and closer to the shelf break relative to the K_1 tide.

However, almost all previous studies have employed either data analysis or numerical modelling methods; thus, theoretical research is lacking. In particular, the existence of amphidromic points in the northeast KS for both diurnal and semidiurnal tides has not been explained based on geophysical dynamics. In this paper, we intend to establish a theoretical model for the K_1 and M_2 tides in the KS-JS basin using the extended Taylor method. The model idealizes the KS-JS basin into three connected uniform-depth rectangular areas, with the effects of bottom friction and Coriolis force included in the governing equations and with the observed tides specified as open boundary conditions. The extended Taylor method enables us to obtain semi-analytical solutions consisting of a series of Kelvin waves and Poincaré modes.

Formatted

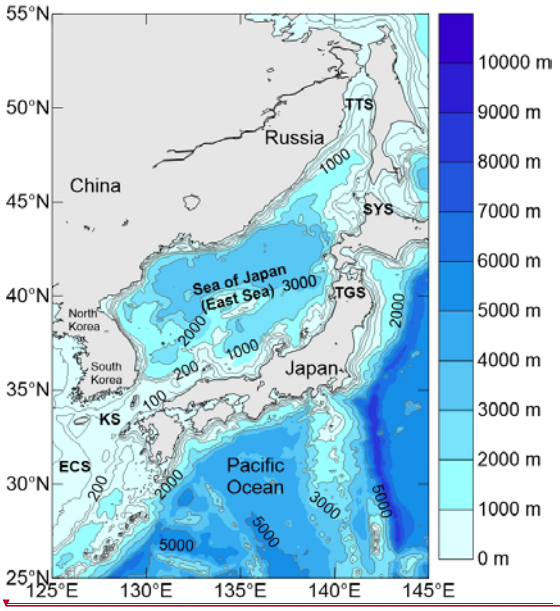

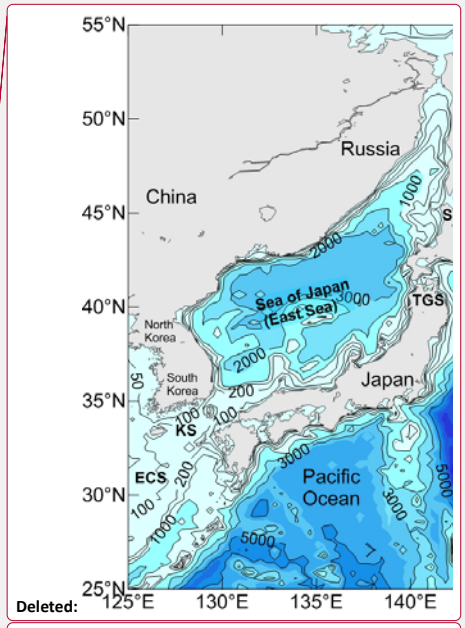

Figure 1: Map of the Korea Strait and its neighbouring areas. (TTS-Tartar Strait, SYS- Soya Strait, TGS- Tsugaru Strait, KS-Korea Strait, ECS-East China Sea). Isobaths are in metres (based on ETOPO1 from US National Geophysical Center).

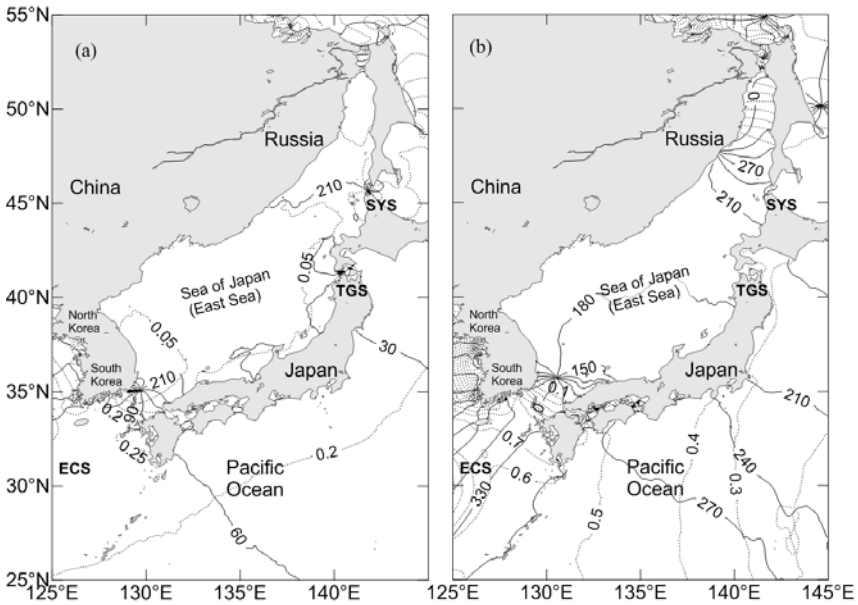

Figure 2: Tidal charts of the KS and its neighbouring areas based on DTU10 (Cheng and Andersen, 2011) for the (a) K1 tide and (b) M2 tide. Solid lines represent the Greenwich phase lag (in degrees), and dashed lines represent amplitude (in metres).

2 The extended Taylor method and its application to multiple rectangular areas

The Taylor problem is a classic tidal dynamic problem (Hendershott and Speranza, 1971). Taylor (1922) first presented a theoretical solution for tides in a semi-infinite rotating rectangular channel of uniform depth to explain the formation of amphidromic systems in gulfs and applied the theory to the North Sea. The classic Taylor problem was subsequently improved by introducing frictional effects (Fang and Wang, 1966; Webb, 1976; Rienecker and Teubner, 1980) and open boundary conditions (Fang et al., 1991) to study tides in multiple rectangular basins (Jung et al., 2005; Roos and Schuttelaars, 2011; Roos et al., 2011) as well as to solve tidal dynamics in a strait (Wu et al., 2018).

The method initiated by Taylor and developed afterwards is called the extended Taylor method (Wu et al., 2018). This method is especially useful in understanding the tidal dynamics in marginal seas and straits because the tidal waves in these sea areas can generally be represented by combinations of the Kelvin waves and Poincaré waves/modes (e. g., Taylor, 1922; Fang and Wang, 1966; Hendershott and Speranza, 1971; Webb, 1976; Fang et al., 1991; Carbajal, 1997; Jung et al., 2005; Roos and Schuttelaars, 2011; Roos et al., 2011; Wu et al., 2018).

2.1 Governing equations and boundary conditions for multiple rectangular areas

A sketch of the model geometry is shown in Fig. 3, and it consists of a sequence of J rectangular areas with length L_j, width W_j and uniform depth h_j for the jth rectangular area (denoted as Areaj, j=1, …, J). For convenience, the shape of the study region shown in Fig. 3 is the same as that for the idealized KS–JS basin, which will be described in the next section. In particular, Area1 represents the KS, which is our focus area in this study.

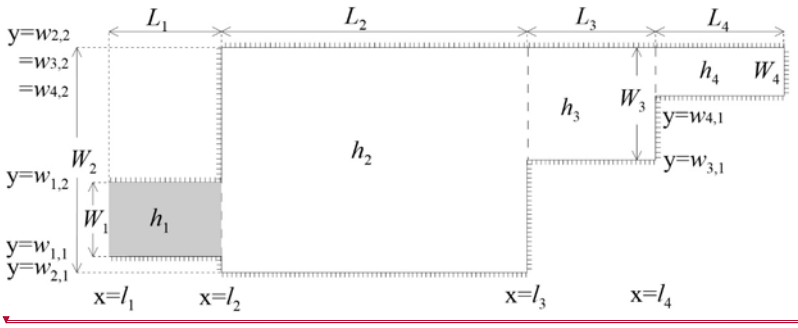

Figure 3: Model geometry.

Consider a tidal wave of angular velocity σ and typical elevation amplitude H. We assume $H/h \ll 1$, and the conservation of momentum and mass leads to the following depth-averaged linear shallow water equations on the f plane:

Deleted: an analytical

Deleted: frequency

Deleted:

$$\begin{cases} \frac{\partial \tilde{u}_j}{\partial t} - f_j \tilde{v}_j = -g \frac{\partial \tilde{\zeta}_j}{\partial x} - \gamma_j \tilde{u}_j \\ \frac{\partial \tilde{v}_j}{\partial t} + f_j \tilde{u}_j = -g \frac{\partial \tilde{\zeta}_j}{\partial y} - \gamma_j \tilde{v}_j \\ \frac{\partial \tilde{\zeta}_j}{\partial t} = -h_j \left[\frac{\partial \tilde{u}_j}{\partial x} + \frac{\partial \tilde{v}_j}{\partial y} \right] \end{cases}, \quad (1)$$

where x and y are coordinates in the longitudinal (along-channel) and transverse (cross-channel) directions; t represents time; $\tilde{u}_j$ and $\tilde{v}_j$ represent the depth-averaged flow velocity components in the x and y directions, respectively, with the subscript j indicating the area number; $\tilde{\zeta}_j$ represents the free surface elevation above the mean level; γ_j represents the frictional coefficient, which is taken as a constant for each tidal constituent in each area; g =9.8 ms^{-2} represents the acceleration due to gravity; and f_j represents the Coriolis parameter, which is also taken as a constant based on the average of the concerned area. The equations in (1) for each j are two-dimensional linearized shallow water equations on an f-plane with momentum advection neglected. For any j, the equations are the same as those used in the work of Taylor (1922) except that bottom friction is now incorporated, such as in Fang and Wang (1966), Webb (1976), Rienecker and Teubner (1980), etc. When a monochromatic wave is considered, $(\tilde{\zeta}_j, \tilde{u}_j, \tilde{v}_j)$ can be expressed as follows:

$$(\tilde{\zeta}_j, \tilde{u}_j, \tilde{v}_j) = \mathrm{Re}(\zeta_j, u_j, v_j) \mathrm{e}^{i\sigma t}, \quad (2)$$

where Re stands for the real part of the complex quantity that follows, (ζ_j, u_j, v_j) are referred to as complex amplitudes of $(\tilde{\zeta}_j, \tilde{u}_j, \tilde{v}_j)$, respectively, $i \equiv \sqrt{-1}$ is the imaginary unit, and σ is the angular velocity of the wave. For this wave, Eq. (1) can be reduced as follows:

$$\begin{cases} (\mu_j + i) u_j - \nu_j v_j = -\frac{g}{\sigma} \frac{\partial \zeta_j}{\partial x} \\ (\mu_j + i) v_j + \nu_j u_j = -\frac{g}{\sigma} \frac{\partial \zeta_j}{\partial y} \\ \zeta_j = \frac{i h_j}{\sigma} \left[\frac{\partial u_j}{\partial x} + \frac{\partial v_j}{\partial y} \right] \end{cases}, \quad (3)$$

in which

$$\mu_j = \frac{\gamma_j}{\sigma} \quad \text{and} \quad \nu_j = \frac{f_j}{\sigma}. \quad (4)$$

Provided that the j-th rectangular area, denoted as Areaj, has a width of W_j, a length of L_j, and ranges from $x = l_j$ to $x = l_{j+1}$ $(l_{j+1} = l_j + L_j)$ in the x direction and from $\mathrm{y} = w_{j,1}$ to $\mathrm{y} = w_{j,2}$ $(w_{j,2} = w_{j,1} + W_j)$ in the y direction, the boundary conditions along the sidewalls within $x \in [l_j, l_{j+1}]$ are taken as follows:

$$v_j = 0 \text{ at } y = w_{j,1} \text{ and } y = w_{j,2}. \quad (5)$$

Along the cross-sections, such as $x = l_j$, various choices of boundary conditions are applicable depending on the problem:

$$u_j = 0, \quad (6)$$

if the cross-section is a closed boundary;

$$u_j = \pm \sqrt{\frac{g}{(1 - i\mu_j) h_j}} \zeta_j, \quad (7)$$

if the free radiation in the positive/negative x direction occurs on the cross-section;

$$\zeta_j = \hat{\zeta}_j, \quad (8)$$

if the tidal elevation is specified as $\hat{\zeta}_j$ along the cross-section; and

$$\begin{cases} \zeta_j = \zeta_{j+1}, \\ u_j h_j = u_{j+1} h_{j+1}, \end{cases} \quad (9)$$

if the cross-section is a connecting boundary of the areas j and $j+1$, with each having a different uniform depth of h_j and h_{j+1}.

Equation (9) is matching conditions accounting for sea level continuity and volume transport continuity. The individual Eqs.

Deleted: the

Deleted: frequency

(6) to (9), or their combination, may be used as boundary conditions for the cross-sections. The relationship between u_j and ζ_j shown in Eq. (7) is based on the solution for progressive Kelvin waves in the presence of friction, which will be given in Eqs. (10) and (11) below.

2.2 General solution

For the *j*-th rectangular area, that is, for $x \in [l_j, l_{j+1}]$ and $y \in [w_{j,1}, w_{j,2}]$, the governing equations in Eq. (3) only have the following four forms satisfying the sidewall boundary condition of Eq. (5) (see, e. g., Fang et al. 1991):

$$\begin{cases} v_{j,1} = 0, \\ u_{j,1} = -a_j \ \exp[\alpha_j y + \mathrm{i}\beta_j (x - l_j)], \\ \zeta_{j,1} = \frac{\beta_j}{\sigma} h_j a_j \exp[\,\alpha_j y + \mathrm{i}\beta_j (x - l_j)]\,; \end{cases} \tag{10}$$

$$\begin{cases} v_{j,2} = 0, \\ u_{j,2} = b_j \ \exp[-\alpha_j y - \mathrm{i}\beta_j (x - l_j)], \\ \zeta_{j,2} = \frac{\beta_j}{\sigma} h b_j \ \exp[-\alpha_j y - \mathrm{i}\beta_j (x - l_j)]\,; \end{cases} \tag{11}$$

$$\begin{cases} v_{j,3} = \sum_{n=1}^{\infty} \kappa_{j,n} \sin r_{j,n} y \exp[-s_{j,n}(x - l_j)], \\ u_{j,3} = \sum_{n=1}^{\infty} \kappa_{j,n} (A_{j,n} \cos r_{j,n} y + B_{j,n} \sin r_{j,n} y) \exp[-s_{j,n}(x - l_j)], \\ \zeta_{j,3} = \frac{ih_j}{\sigma} \sum_{n=1}^{\infty} \kappa_{j,n} (C_{j,n} \cos r_{j,n} y + D_{1,n} \sin r_{j,n} y) \exp[-s_{j,n}(x - l_j)]; \end{cases} \tag{12}$$

and

$$\begin{cases} v_{j,4} = \sum_{n=1}^{\infty} \lambda_{j,n} \sin r_{j,n} y \exp[-s_{j,n}(l_{j+1} - x)], \\ u_{j,4} = \sum_{n=1}^{\infty} \lambda_{j,n} (A'_{j,n} \cos r_{j,n} y + B'_{j,n} \sin r_{j,n} y) \exp[-s_{j,n}(l_{j+1} - x)], \\ \zeta_{j,4} = \frac{ih_j}{\sigma} \sum_{n=1}^{\infty} \lambda_{j,n} (C'_{j,n} \cos r_{j,n} y + D'_{j,n} \sin r_{j,n} y) \exp[-s_{j,n}(l_{j+1} - x)]. \end{cases} \tag{13}$$

where α_j, β_j, $r_{j,n}$ and $s_{j,n}$ are equal to the following:

$$\alpha_j = \frac{\nu_j}{(1 - \mathrm{i}\mu_j)^{1/2}} k_j, \tag{14}$$

$$\beta_j = (1 - i\mu_j)^{1/2} k_j, \tag{15}$$

$$r_{j,n} = \frac{n\pi}{W_j}\ , \tag{16}$$

and

$$s_{j,n} = (r_{j,n}^2 + \alpha_j^2 - \beta_j^2)^{\frac{1}{2}}, \tag{17}$$

in which $k_j = \sigma / c_j$ is the wave number, with $c_j = \sqrt{gh_j}$ being the wave speed of the Kelvin wave in the absence of friction. The parameters $s_{j,n}$ in Eq. (17) are of fundamental importance in determining the characteristic of the Poincaré modes. If $\mathrm{Re}(\beta_j^2 - \alpha_j^2)^{1/2} < \pi / W_j$, all Poincaré modes are bound in the vicinity of the open, connecting or closed cross-sections (see Fang and Wang, 1966; Hendershott and Speranza, 1971 for in absence of friction); while if $\mathrm{Re}(\beta_j^2 - \alpha_j^2)^{1/2} > n\pi / W_j$, the *n*-th and lower-order Poincaré modes are propagating waves. In the present study, the inequality $\mathrm{Re}(\beta_j^2 - \alpha_j^2)^{1/2} < \pi / W_j$ holds for all rectangular areas shown in Fig.3, so that all Poincaré modes in the present study appear in a bound form. The parameter

Deleted: both the idealized KS and JS

$s_{j,n}$ has two complex values for each n, and here,we choose the one that has a positive real part. To satisfy the equations in Eq. (3), $(A_{j,n}, B_{j,n}, C_{j,n}, D_{j,n})$ and $(A'_{j,n}, B'_{j,n}, C'_{j,n}, D'_{j,n})$ should be as follows:

$$A_{j,n} = \frac{\left[(\mu_j+i)^2+\nu_j^2\right] r_{j,n} s_{j,n}}{(\mu_j+i)^2 r_{j,n}^2+\nu_j^2 s_{j,n}^2} s_{j,n}, \quad (18)$$

$$B_{j,n} = \frac{\nu_j(\mu_j+i)\left(\alpha_j^2-\beta_j^2\right)}{(\mu_j+i)^2 r_{j,n}^2+\nu_j^2 s_{j,n}^2}, \quad (19)$$

$$C_{j,n} = r_{j,n} - s_{j,n} A_{j,n}, \quad (20)$$

$$D_{j,n} = -s_{j,n} B_{j,n}, \quad (21)$$

$$A'_{j,n} = -A_{j,n}, \quad (22)$$

$$B'_{j,n} = B_{j,n}, \quad (23)$$

$$C'_{j,n} = C_{j,n}, \quad (24)$$

and

$$D'_{j,n} = -D_{j,n} \quad (25)$$

Equations (10) and (11) represent Kelvin waves propagating in the $-x$ and x directions, respectively; and Eqs. (12) and (13) represent two families of Poincaré modes bound along the cross-sections $x = l_j$ and l_{j+1} in the *j*-th rectangular area, respectively. Coefficients $(a_j, b_j, \kappa_{j,n}, \lambda_{j,n})$ determine amplitudes and phase lags of Kelvin waves and Poincaré modes. These coefficients must be chosen to satisfy the boundary conditions, using preferably the collocation approach.

2.3 Defant's collocation approach

The collocation approach was first proposed by Defant in 1925 (see Defant, 1961), and is convenient in determining the coefficients $(a_j, b_j, \kappa_{j,n}, \lambda_{j,n})$. In the simplest case, that is, if the model domain contains only a single rectangular area, then J =1 and the index *j* has only one value: $j = 1$, the calculation procedure can be as follows. First, we truncate each of the two families of Poincaré modes in Eqs. (12) and (13) at the N_1-th order so that the number of undetermined coefficients for two families of Poincaré modes is $2N_1$ and the total number of undetermined coefficients (plus those for a pair of Kelvin waves) is thus $2N_1 + 2$. To determine these unknowns, we take equally spaced $N_1 + 1$ dots, which are called collocation points, located at $y = w_{1,1} + \frac{W_1}{2(N_1+1)}$, $w_{1,1} + \frac{3W_1}{2(N_1+1)}$, ... , $w_{1,1} + \frac{(2N_1+1)W_1}{2(N_1+1)}$ on both cross-sections $x = l_1$ and l_2. At these points, one of the boundary conditions given by Eqs. (6) to (8) should be satisfied, which yields $2N_1 + 2$ equations. By solving this system of equations, we can obtain $2N_1 + 2$ coefficients $(a_1, b_1, \kappa_{1,n}, \lambda_{1,n})$. Because the high-order Poincaré modes, which have great values of *n* and $s_{1,n}$ in Eqs. (12) and (13), decay from the boundary very quickly, it is generally necessary to retain only a few lower-order terms. In the above single-rectangle case, the spacing of collocation points is equal to $\Delta y = W_1/(N_1 + 1)$.

For $J > 1$, that is, the model contains multiple rectangular areas connected one by one, we can treat the approach in the

following way. First, we may choose a common divisor of $W_1, W_2, \dots, W_J$ as a common spacing, which is denoted by Δy, for all areas. For the jth rectangle (Fig. 3), we may select the collocation points at $y = w_{j,1} + \frac{\Delta y}{2}, w_{j,1} + \frac{3\Delta y}{2}, \dots, w_{j,2} - \frac{\Delta y}{2}$ on the cross-sections $x = l_j$ and $x = l_{j+1}$, where $w_{j,2} = w_{j,1} + W_j$. The number of collocation points on each cross-section in this area is equal to $W_j/\Delta y$. Thus the number of undetermined coefficients for the Poincaré modes is selected to be $N_j = (W_j/\Delta y) - 1$. Accordingly, there will be in total $\sum_{j=1}^{J}(2N_j + 2)$ collocation points in J areas. Note that on the cross-section connecting Area$j$ and Area(j+1), the collocation points that belong to Area$j$ and those that belong to Area(j+1) are located at the same positions. For the points located on the open or closed boundaries, Eqs. (6) to (8) are applicable, while for the points located on the cross-sections connecting two areas, Eq. (9) should be applied. From these $\sum_{j=1}^{J}(2N_j + 2)$ equations, we can obtain $\sum_{j=1}^{J}(2N_j + 2)$ coefficients $(a_j, b_j, \kappa_{j,n}, \lambda_{j,n})$, in which $j = 1, 2, \dots, J$ and $n = 1, 2, \dots N_j$.

3 Tidal dynamics of the Korea Strait

As noted by Odamaki (1989b), the co-oscillating tides are dominant in the JS, which is mainly induced by inputs at the opening of the KS rather than those through the TGS and SYS. Furthermore, our study focuses on the KS, in which influences of the tide-generating force and the inputs from the TGS and SYS are negligible. Therefore, we idealize the KS-JS basin as a semi-enclosed basin with a sole opening connected to the ECS and study the co-oscillating tides generated by the tidal waves from the ECS through the opening.

3.1 Model configuration and parameters for the Korea Strait and Japan Sea

To establish an idealized analytical model for the KS–JS basin, we use four rectangular areas as shown in Fig. 4 to represent the study region. The first rectangle, designated as Area1, represents the KS, which is our focus area. According to the shape of its coastline, we use three rectangles designated as Area2 and Area3 to represent the JS. We place the x-axis parallel to but 200 km away from the southeast sidewall of the KS (that is, $w_{1,1}$ in Fig. 3 is equal to 200 km), and the y-axis is in the direction perpendicular to the x-axis through the opening of the KS (Fig. 4). The selected depths are the mean depths calculated based on the topographic dataset ETOPO1. The K_1 and M_2 angular velocities are equal to $7.2867 \times 10^{-5}\text{s}^{-1}$ and $1.4052 \times 10^{-4}\text{s}^{-1}$, respectively. The details of the model parameters can be found in Table 1.

Deleted: three

Deleted: area of

Deleted: two

Deleted: frequencies

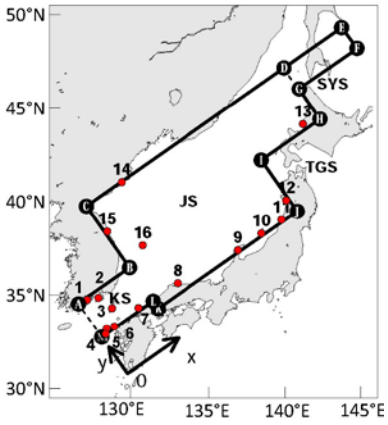

Figure 4: Idealized model domain fitting the Korea Strait and Japan Sea. The dashed line represents open boundary, and the solid lines represent closed boundaries. A, B, … ,M indicate the localities of the points used in Fig. 6 for model-observation comparison. Numbered red dots are tidal gauge stations where the observed harmonic constants are used for model validation in Table 2.

Based on the depths listed in Table 1, the wavelengths of the K_1 Kelvin waves in these four areas are 2686 km, 12189 km, 11398 km, and 2561 km, respectively, and those of the M_2 Kelvin waves are 1393 km, 6321 km, 5911 km and 1328 km, respectively. Because the widths of the areas are all smaller than half the corresponding Kelvin wavelengths, the inequality $\mathrm{Re}(\beta_j^2 - \alpha_j^2) < \pi/W_j$ as stated in the subsection 2.2 is satisfied (see also Godin, 1965; Fang and Wang, 1966; Wu et al., 2018), Thus the Poincaré modes can only exist in a bound form.

Table 1. Parameters used in the model.

Parameter	Area1	Area2	Area3	Area4
W_j (km)	230	700	350	140
L_j (km)	350	950	400	400
$w_{j,1}$ (km)	250	200	550	760
f_j ($10^{-5}s^{-1}$)	8.28	9.24	10.10	10.65
h_j (m)	99	2039	1783	90
N_j	22	69	34	13

In addition to the parameters listed in Table 1, we need to estimate the parameters μ_{M_2} and μ_{K_1} as defined by Eq. (4). Since M_2 has the largest tidal current in the KS (Teague et al., 2001), and we assume that the tidal currents are rectilinear, the linearized frictional coefficient for M_2 is approximately equal to the following, after Pingree and Griffiths (1981), Fang (1987)

Deleted:

Deleted: J

Deleted: three

Deleted: and

Deleted: and

Deleted:

Inserted Cells

and Inoue and Garrett (2007),

$$\gamma_{M_2} \approx \frac{C_D}{h}\frac{8}{3\pi}U_{M_2}\left(1+\frac{3}{4}\sum_{i=2,3,\ldots}\epsilon_i^2\right) , \quad (26)$$

where C_D is the drag coefficient and U_{M_2} is the tidal current amplitude of M_2, $\epsilon_i = U_i/U_{M_2}$, with U_i representing the tidal current amplitude of the constituent i (here, we designate i=1 for M_2 and i=2, 3, … for any constituents other than M_2). According to Fang (1987) and Inoue and Garrett (2007), the linearized frictional coefficient for the non-dominant constituent i is approximately equal to the following:

$$\gamma_i \approx \frac{C_D}{h}\frac{4}{\pi}U_{M_2}\left(1+\frac{\epsilon_i^2}{8}+\frac{1}{4}\sum_{k=2,3,\ldots,k\neq i}\epsilon_k^2\right) , \quad (27)$$

Inserting Eqs. (26) and (27) into Eq. (4), we can obtain the parameter μ. Teague et al. (2001) provided tidal current harmonic constants at 10 mooring stations along two cross-sections in the KS. The averaged values of the major semi-axes of the tidal current ellipses at these stations are 0.154, 0.119, 0.101 and 0.062 m/s for M_2, K_1, O_1 and S_2, respectively. Here, we use these values and $C_D \approx 0.0026$ to estimate the parameters in Eqs. (26) and (27). Then, after inserting these values into Eq. (4), we obtain rough estimates of μ_{M_2} and μ_{K_1} for the KS (Area1), which are approximately 0.05 and 0.09, respectively. Since the JS is much deeper and has much weaker tidal currents than the KS, we simply let $\mu_{K_1} = \mu_{M_2} = 0$ for both Area2 and Area3.

For the collocation approach, we take 10 km as the spacing between collocation points. Thus in this model, a total of 198 collocation points are used to establish 256 equations, and the parameters of 3 pairs of Kelvin waves and 125 pairs of Poincaré modes can be obtained. Along the open boundary of the KS, the open boundary condition Eq. (8) is employed, with the value of $\hat{\zeta}$ equal to the observed harmonic constants from the global tide model DTU10 (Cheng and Anderson, 2011). Along the cross-sections connecting Area1 with Area2 and Area2 with Area3, the matching conditions Eq. (9) are applied. Along the solid cross-sections, condition Eq. (6) is used.

3.2 Model results and validation

The obtained analytical solutions of the K_1 and M_2 tides using the extended Taylor method are shown in Fig.5a and 5b, respectively. The maximum amplitude of the K_1 tide is 0.34 m, which appears at the southwest corner of the KS. The amplitude decreases from southwest to northeast, and a counter-clockwise tidal wave system occurs in the northeast part of the KS, with amplitudes less than 0.05 m near the amphidromic point. A co-tidal line with a phase lag of 210° runs from the amphidromic point in the KS into the southwest JS.

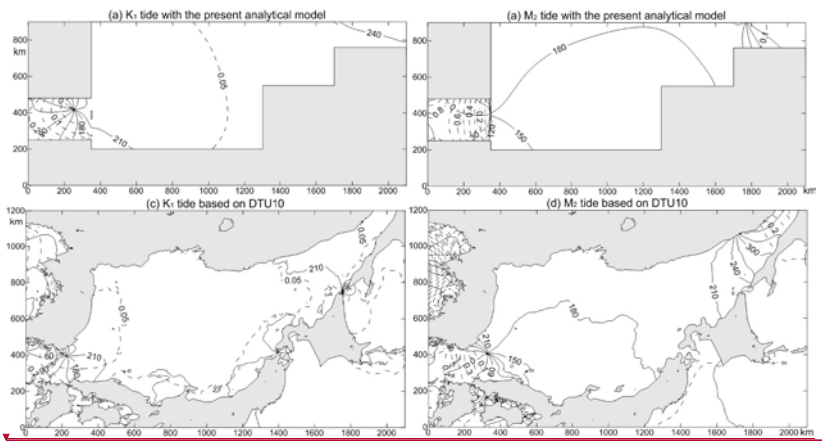

Figure 5: Comparison of tidal system charts. (a) K_1 and (b) M_2 tides from the present theoretical model; and (c) K_1 and (d) M_2 tides from DTU10 (Chen and Andersen, 2011).

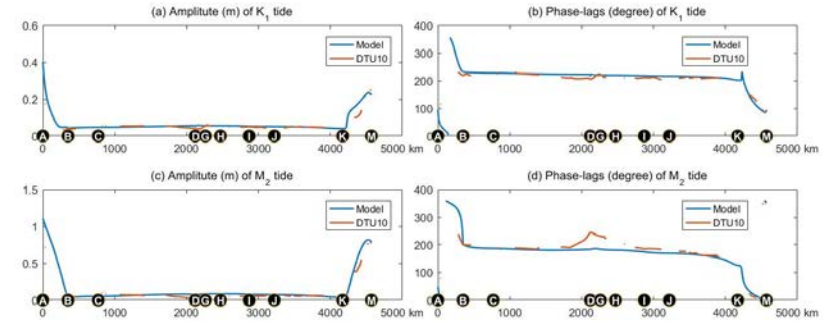

Figure 6: Comparison of model results (blue) and observations based on DTU10 (orange) along the coasts. (a) K_1 amplitudes; (b) K_1 phase lags; (c) M_2 amplitudes; and (d) M_2 phase lags. The locations of the points A, B, C, D, G, H, I, J, K, L, M are shown in Fig. 4.

The maximum amplitude of the M_2 tide is 1.02 m, which appears at the westernmost corner of the KS. The amplitude decreases gradually from southwest to northeast along the direction of the strait, and the amphidromic point occurs at the junction of the KS and JS. The amplitudes near the amphidromic point are lower than 0.1 m, and the phase lags in the most part of the JS vary from 150° to 210°. A degenerated amphidromic point appears near the entrance of the Tartar Strait. The comparison with the tidal charts based on data from DTU10 (Fig.5c, d) shows that the model-produced tidal systems agree fairly well with the observations.

To quantitatively validate the model results, we first extract the data along the solid boundary of the model for comparison as shown in Fig.6. For the K_1 tide, the model-produced amplitudes and phase lags along the boundary in the JS both agree well

Deleted:

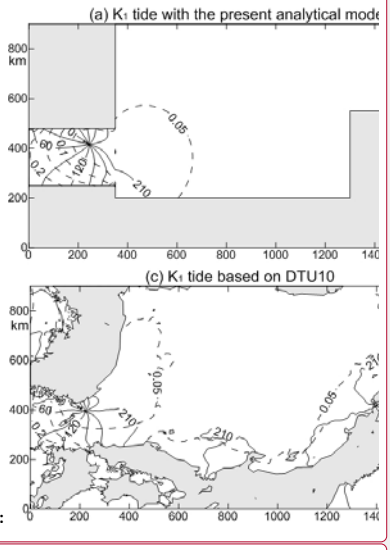

Deleted: analytical

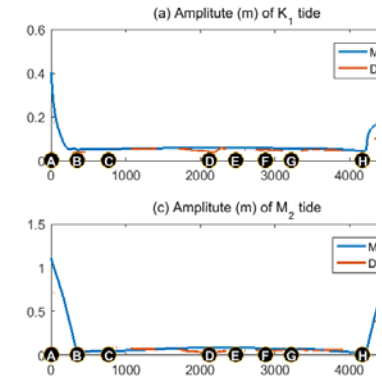

Deleted:

Deleted: …

Deleted: are

with the observed data, although small differences occur at the northern corner of the JS. For the M_2 tide, the greatest phase-lag errors are approximately 64° near the entrance of the Tartar Strait due to the existence of a degenerated amphidromic point near this area (Fig. 2b).

For further validation, we select 16 tide gauge stations where harmonic constants are available from the International Hydrographic Bureau (1930). The station locations are shown in Fig. 4. The result of the comparison is given in Table 2, which also shows that the model results are consistent with the data obtained from gauge observations: the RMS (root mean square) differences of amplitudes of K_1 and M_2 are 0.014 and 0.032 m, respectively; and those of the phase lags are 7.0° and 5.2°, respectively.

Table 2. Comparison between harmonic constants from the observations and models at coastal tide gauge stations.

		K_1				M_2			
No	Station Name	Amplitude (m)		Phase lag (°)		Amplitude (m)		Phase lag (°)	
		Obs	model	obs	model	obs	model	obs	model
1	Reisui Ko	0.21	0.20	50	39	1.02	0.93	357	10
2	Toei Ko	0.16	0.12	46	39	0.80	0.76	355	2
3	Takesiki Ko, Aso Wan	0.12	0.11	83	87	0.66	0.66	1	6
4	Aokata	0.23	0.23	90	85	0.80	0.81	356	358
5	Konoura, Uku Sima	0.20	0.22	92	88	0.78	0.79	354	2
6	Usuka Wan, Hirado Sima	0.19	0.21	102	97	0.74	0.78	2	8
7	Kottoi	0.12	0.13	174	155	0.32	0.34	31	33
8	Sitirui	0.04	0.04	206	211	0.06	0.04	152	148
9	Nakai Iri,Hoku Wan	0.06	0.05	215	214	0.07	0.07	172	164
10	Ryotu Ko, Sado	0.05	0.05	211	215	0.05	0.07	181	167
11	Kamo Ko	0.06	0.05	211	216	0.07	0.07	174	169
12	Akita	0.06	0.05	220	216	0.05	0.07	174	170
13	Hamamasu	0.05	0.06	211	219	0.05	0.09	185	180
14	Zyosin Ko	0.06	0.05	227	227	0.08	0.06	187	185
15	Sokcho	0.04	0.05	236	228	0.07	0.05	189	188
16	Uturyo To	0.04	0.04	222	226	0.04	0.04	194	180
	RMS difference	0.014		7.0		0.032		5.2	

Although the theoretical model greatly simplifies the topography and boundary, the amplitude and phase-lag differences of

Deleted: 70° at…4° near the northernmost corner…ntrance of …
Deleted: 031…32 m, respectively; and those of the phase la …
Deleted: obs
Deleted: 38
Deleted: 11
Deleted: 38
Deleted: 77
Deleted: 7
Deleted: 157
Deleted: 33
Deleted: 32
Deleted: 05
Deleted: 213
Deleted: 03
Deleted: 156
Deleted: 216
Deleted: 06
Deleted: 169
Deleted: 06
Deleted: 217
Deleted: 06
Deleted: 172
Deleted: 06
Deleted: 217
Deleted: 173
Deleted: 06
Deleted: 217
Deleted: 174
Deleted: 220
Deleted: 08
Deleted: 179
Deleted: 226
Deleted: 05
Deleted: 194
Deleted: 199
Deleted: 05
Deleted: 193
Deleted: 4
Deleted: 031
Deleted: 6.4
Formatted: Indent: First line: 1 ch

these two tidal constituents are very small in the KS and its surroundings and the basic characteristics of the tidal patterns are well retained (Fig. 5). These findings show that the simplification of the model is reasonable and the extended Taylor method is appropriate for modelling the tides in the KS-JS basin. Therefore, it is meaningful to use the model results for theoretical analysis.

3.3 Tidal waves in the Korea Strait

To reveal the relative importance of the Kelvin waves versus Poincaré modes in the modelled Korea Strait, the superposition of Kelvin waves and that of the Poincaré modes are given in the upper panels of Fig.7 for K_1 and in the upper panels of Fig.8 for M_2.

For the K_1 tide in the KS, the superposition of the incident (northeastward) and the reflected (southwestward) Kelvin waves appears as a counter-clockwise amphidromic system, with the amphidromic point located near the middle of the strait, but closer to the southeast coast of Korea (Fig.7a). The highest amplitude of the superposed Kelvin waves is 0.3 m, and the mean difference from the observations is less than 0.03 m. The superposition of all Poincaré modes has amplitudes of approximately 0.1 m near the cross-sections on both left and right sides, and a counter-clockwise amphidromic point exists nearly at the centre of the strait (Fig. 7b). Since the amplitudes of the superposed Poincaré modes are significantly smaller than those of the superposed Kelvin waves, the latter can basically represent the total tidal pattern, including the counter-clockwise amphidromic system.

For the M_2 tide, the highest amplitude of the superposition of two Kelvin waves is approximately 0.95 m, which appears at the southwest corner of the strait (Fig. 8a). The amplitude decreases from southwest to northeast along the strait, and the amphidromic point appears near the cross-section connecting to the JS, where a topographic step exists. The maximum deviation of the amplitudes of the superposed Kelvin waves from the observations is 0.06 m, and the structure of the superposed Kelvin waves is consistent with the observation. The amplitudes of the superposed Poincaré modes are generally less than 0.2 m on both left and right sides of the KS, and they decay rapidly towards the middle of the strait, thus forming a counter-clockwise amphidromic system structure (Fig. 8b). Therefore, the M_2 tide in the KS is also mainly controlled by Kelvin waves.

The above results show that the Poincaré modes only exist along the open boundary and the connecting cross-section and their amplitudes quickly approach to zero away from these cross-sections. In fact, these properties of the Poincaré wave are inherent in any narrow strait. Therefore, in the following, we will focus on Kelvin waves and analyze the characteristics of the incident (northeastward) and reflected (southwestward) Kelvin waves.

The incident and reflected K_1 Kelvin waves are shown in Figs. 7c and 7d, respectively. The area-mean amplitude of the incident Kelvin wave in the KS is 0.248 m, and that of the reflected Kelvin wave is 0.190 m, which is 77% of the incident Kelvin wave. On the connecting cross-section, the section-mean amplitude of the incident Kelvin wave is 0.243 m, and the

Deleted: 96

Deleted: 253

Deleted: 196

Deleted: 249

section-mean phase lag is 151.6°. The section-mean amplitude of the reflected Kelvin wave is 0.194 m, which is 80% of the incident Kelvin wave. The section-mean phase lag is 295.8°, indicating that the phase lag increases by 144.2° when the wave is reflected. The amphidromic point of the superposed Kelvin wave is 137 km away from the step and close to the northwest shore of the KS.

The incident and reflected M_2 Kelvin waves are shown in Figs. 8c and 8d, respectively. The area-mean amplitude of the incident Kelvin wave in the KS is 0.471 m, and that of the reflected Kelvin wave is 0.439 m, which is 93% of the incident Kelvin wave. This ratio is larger than the K_1 tide because the bottom friction of M_2 is smaller and less energy is lost in the propagation process. On the connecting cross-section, the mean amplitude of the incident Kelvin wave is 0.462 m, and the phase lag is 97.9°. The mean amplitude of the reflected Kelvin wave is 0.447 m, which is 97% of the incident Kelvin wave, and the phase lag is approximately 266.4°, with a phase-lag increase of 168.5°, which is closer to 180° as compared to the corresponding value of the K_1 tide. Accordingly, the M_2 amphidromic point of the superposed Kelvin wave shifts to approximately 21 km away from the step. A comparison between Fig. 7a and Fig. 8a shows that the amphidromic point of K_1 is located west of that of M_2. This result reproduces well the observed phenomenon as seen from Fig. 2.

The above results indicate that the relation of the amplitudes and phase lags of the reflected Kelvin wave with the incident wave plays a decisive role in the tidal system in the KS, especially in the formation of amphidromic points, for both the K_1 and M_2 tides.

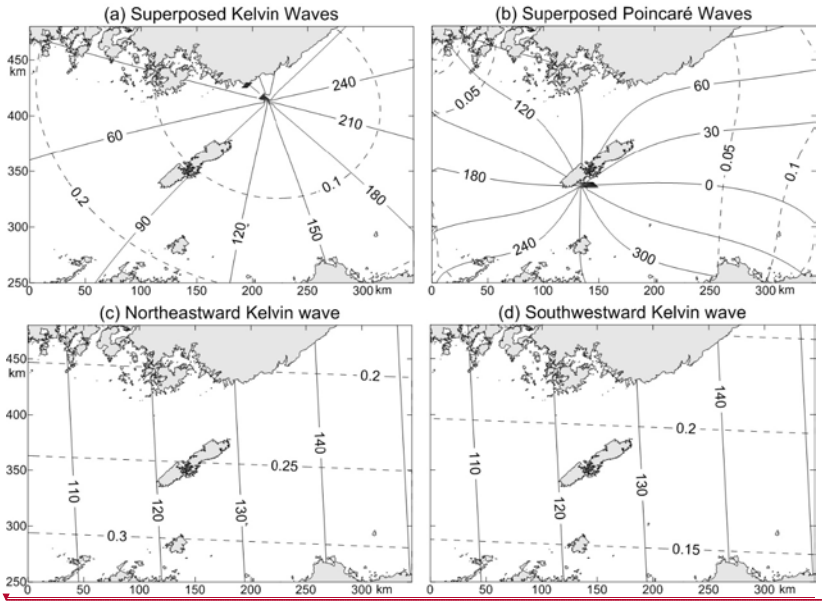

Figure 7: Decomposed charts for the model-produced K_1 tide in the Korea Strait: (a) contribution of Kelvin waves; (b) contribution of Poincaré modes; (c) northeastward (incident) Kelvin wave; and (d) southwestward (reflected) Kelvin wave.

Deleted: 3
Deleted: 199
Deleted: 294.2
Deleted: 142.9
Deleted: 145
Deleted: 466
Deleted: 443
Deleted: 95
Deleted: 457 cm
Deleted: 7
Deleted: 452
Deleted: 99
Deleted: 8
Deleted: 169.1
Deleted: 20

Deleted:

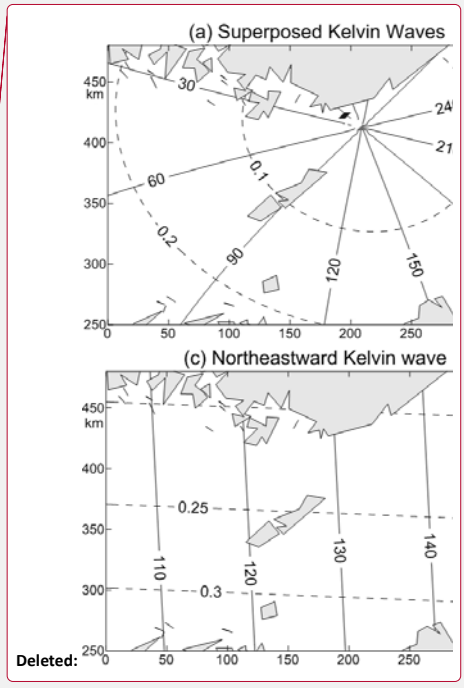

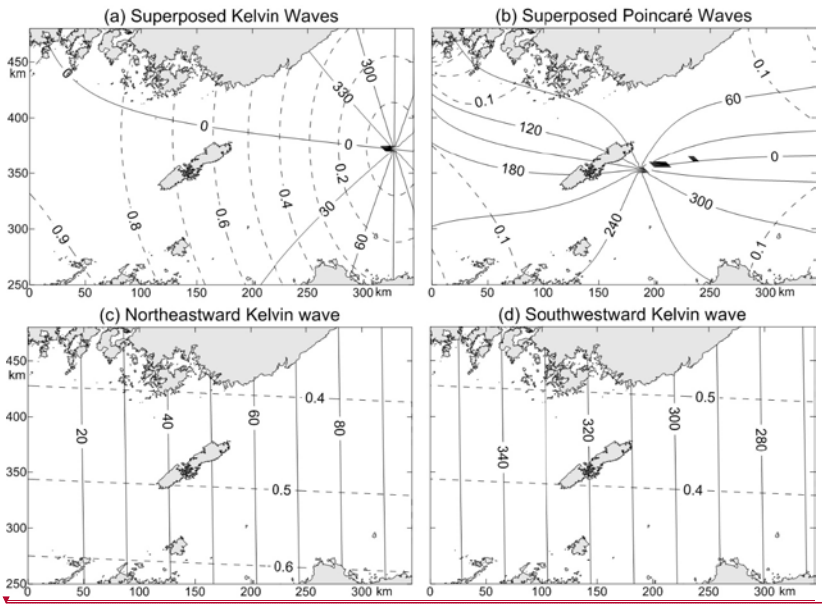

Figure 8: Same as in Fig. 7 but for M_2.

Deleted:

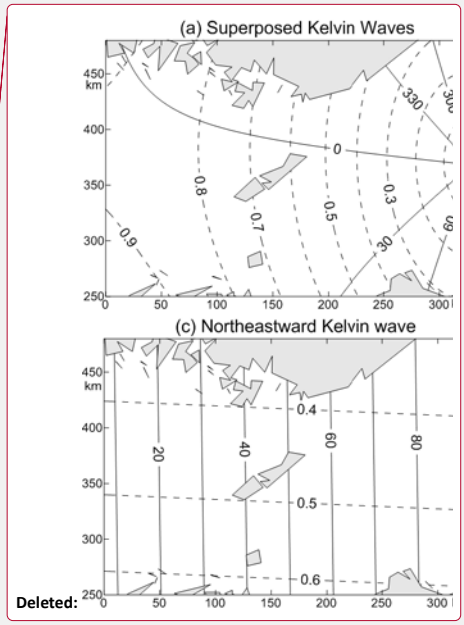

4 Discussion on the formation mechanism of amphidromic points

To explore the tidal dynamics of the KS–JS basin, especially the formation mechanism of amphidromic points, we consider the simplest case: a one-dimensional tidal model in channels. In the one-dimensional case, the amphidromic point is equivalent to the wave node. As previously mentioned, an important feature of the topography of the KS–JS basin is that there is a steep continental slope between the KS and JS, and to northeast of this slope, the JS is much deeper and wider than the KS. Thus, the channel is idealized to contain two areas, with the first one (Area1) having uniform depth h_1 and uniform width W_1 and the second one (Area2) having uniform depth h_2 and uniform width W_2. Therefore, the idealized channel contains abrupt changes in depth and width at the connection of these two areas. An incident wave enters the first area and propagates toward the second area passing over the topographic step. For simplicity, we neglect friction.

If the second area is semi-infinitely long, allowing for the wave radiating out from the second area freely, then a part of the wave is reflected at the connecting point and another part is transmitted into the second area. The amplitude of the transmitted wave is (see e. g. Dean and Dalrymple (1984))

$$H_T = \kappa_T H_I, \tag{28}$$

where H_I is the amplitude of the incident wave and κ_T is called the transmission coefficient, which is equal to

$$\kappa_T = \frac{2}{1+\rho}, \tag{29}$$

Deleted: sharp

Deleted: Dean and Dalrymple (1984) have presented a solution

Deleted: a tidal waves travelling in such a channel; however, in their study,

Deleted: was allowed to radiate

Deleted: which implies that the second area is assumed to be semi-infinitely long. Their solution shows that

where

$$\rho = \frac{c_2 W_2}{c_1 W_1} = \frac{\sqrt{h_2} W_2}{\sqrt{h_1} W_1} \tag{30}$$

with $c_j = \sqrt{g h_j}$ representing the wave speed in the j-th area, $j = 1, 2$. c_j is in fact proportional to $\sqrt{h_j}$. The amplitude of the reflected wave H_R is

$$H_R = \kappa_R H_I \tag{31}$$

where κ_R is called the reflection coefficient, and is equal to the following:

$$\kappa_R = \frac{1-\rho}{1+\rho} \tag{32}$$

If $\rho > 1$, namely, if $\sqrt{h_2} W_2 > \sqrt{h_1} W_1$, then $\kappa_R < 0$, (32) can be rewritten in the form

$$\kappa_R = \frac{\rho-1}{\rho+1} \exp(-i\pi). \tag{33}$$

The above equation indicates that at the connecting point, the reflected wave changes its phase lag by 180°. Therefore, the superposition of incident and reflected waves in Area1 has the minimum amplitude at the connecting point. This theory explains how the reflected wave can be generated by abrupt increases in water depth and basin width, and why the reflected wave there has a phase lag opposite to the incident wave.

The complete solution for this case is as follows (see also Dean and Dalrymple (1984)):

Deleted: Appendix for derivation):

$$\begin{cases} \zeta(x) = H_I \left(\exp\{-i[k_1(x-l_1)+\theta_1]\} + \frac{\rho-1}{\rho+1} \exp\{-i[-k_1(x-l_1)+2\chi_1+\theta_1+\pi]\} \right), & l_1 \ll x \ll l_2 \\ \zeta(x) = \frac{2}{1+\rho} H_I \exp\{-i[k_2(x-l_2)+\chi_1+\theta_1]\}, & l_2 \ll x \end{cases} \tag{34}$$

where θ_1 represents the phase lag of the incident wave at the opening of Area1; $k_j = \sigma / c_j$ is the wave number, with $c_j = \sqrt{g h_j}$ representing the wave speed in Areaj, j=1, 2; and $\chi_1 = k_1 L_1$. This solution for the K_1 and M_2 constituents for h_1=99 m, L_1=350 km, W_1=230 km, h_2=2039 m, and W_2=700 km is plotted with the blue curves in Fig. 9.

However, Sect. 3.3 shows that the phase-lag changes of the reflected waves relative to the incident waves are not exactly equal to 180° but rather are smaller than 180°, and the discrepancy increases with the decreasing angular frequency. To explain this discrepancy, we improve the above theory by introducing the reflected wave in the second area. In fact, the JS is represented with a semi-closed area in the two-dimensional model (Sect. 3.1), namely, all boundaries except those connected to KS are solid ones (Fig. 4). Therefore, in the following one-dimensional model, the second area is closed at its right end so that the reflection will occur at this end. In this case, the solution becomes more complicated and is dependent on the length of the second area L_2. The reflection coefficient κ_R now has the following form (see supplement for derivation):

Deleted: Appendix

$$\kappa_R = \exp(-i2\delta). \tag{35}$$

in which δ is determined by the following equations:

$$\begin{cases} \cos\delta = \frac{1+\cos 2\chi_2}{[(1+\cos 2\chi_2)^2+(\rho \sin 2\chi_2)^2]^{1/2}}, \\ \sin\ \delta = \frac{\rho \sin 2\chi_2}{[(1+\cos 2\chi_2)^2+(\rho \sin 2\chi_2)^2]^{1/2}}, \end{cases} \quad (36)$$

where $\chi_2 = k_2 L_2$. Eq. (36) indicates that the length, width and depth of Area2 are also important in determining the phase-lag increase of the reflected wave relative to the incident wave in Area1.

The complete solution for this case is as follows:

$$\begin{cases} \zeta(x) = H_I(\exp\{-i[k_1(x-l_1)+\theta_1]\} + \exp\{-i[-k_1(x-l_1)+2\chi_1+\theta_1+2\delta]\}), & l_1 \ll x \ll l_2 \\ \zeta(x) = \epsilon H_I(\exp\{-i[k_2(x-l_2)+(\chi_1+\phi+\theta_1)]\} + \exp\{-i[-k_2(x-l_2)+(2\chi_2+\chi_1+\phi+\theta_1)]\}), & l_2 \ll x \ll l_3 \end{cases} \quad (37)$$

where $\varepsilon = 2E^{-1}$. E and ϕ are determined by the following relations:

$$\begin{cases} E\cos\phi = (\rho+1) - (\rho-1)\cos 2\chi_2, \\ E\cos\phi = (\rho-1)\sin 2\chi_2. \end{cases} \quad (38)$$

The first terms on the rhs (right-hand side) of the two equations in Eq. (37) represent the waves propagating in the positive x direction, and the second terms are those propagating in the negative x direction. This solution for the K_1 and M_2 constituents for the case h_1=99 m, L_1=350 km, W_1=230 km, h_2=2039 m, L_2=1150 km, and W_2=700 km is plotted with the red curves in Fig. 9.

Equation (35) indicates that the amplitude of the reflected wave in the first area is equal to that of the incident wave. This result is natural because friction is not considered and no dissipation is present during wave propagation. Equation (35) also indicates that the phase lag of the reflected wave at the connecting point is greater than that of the incident wave at the same point by 2δ. Since the node of the superposition of the incident and reflected waves appears at the place where the phase lags of these two waves are opposite, the first node should appear at Δx away from the connecting point with

$$\Delta x = (\pi - 2\delta)/(2k_1). \quad (39)$$

The above relationship can also be obtained from the first equation of Eq. (37). The dependence of 2δ on σ for the case h_1=99 m, L_1=350 km, W_1=230 km, h_2=2039 m, L_2=1150 km, and W_2=700 km is plotted in Fig. 10. This figure shows that $2\delta = 0$ when $\sigma = 0$ and 2δ increases with increasing σ, although it is always less than 180°. In particular, $2\delta = 167.7°$ when $\sigma = \sigma_{K_1}$ and $2\delta = 176.2°$ when $\sigma = \sigma_{M_2}$. Based on this theory, the M_2 and K_1 amphidromic points should be located at 7.4 and 45.9 km away from the connecting point, respectively. Compared with the two-dimensional model results given in Sect. 3.3, this theory roughly explains one third of the changes. The remaining two third of the changes may be due to the effect of Coriolis force. The solution of phase-lag changes at the cross-section in the two-dimensional rotating basin involves interactions among three Kelvin waves (an incident and a reflected Kelvin waves in Area1 and a transmitted Kelvin wave in Area2) and two families of Poincaré modes at the connecting cross-section (one family in each area). Taylor (1922), Fang and Wang (1966), and Thiebaux (1988) have studied the Kelvin-wave reflection at the closed cross-section of semi-infinite rotating two-dimensional channels. In their studies, only two Kelvin waves and one family of Poincaré modes were involved. In

Moved (insertion) [1]

Formatted: Indent: First line: 1 ch

Deleted: can

Deleted: attributed

comparison to their studies, the present problem is much more complicated. Because of the complexity of the problem, we will presently leave it for a future study.

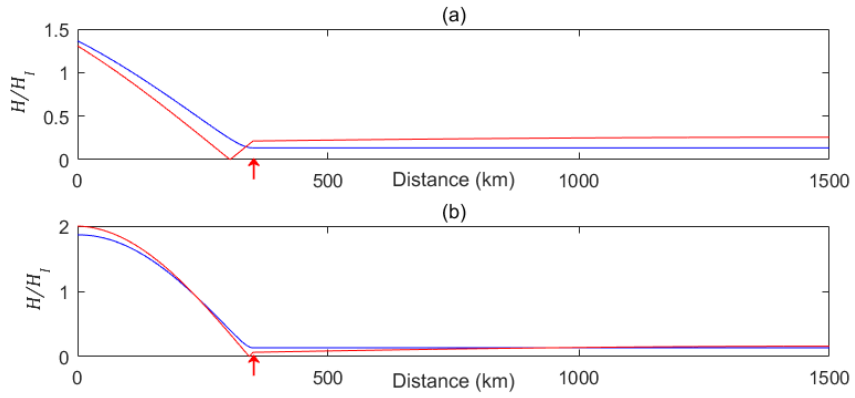

Figure 9: Amplitude distribution along the channel. (a) K_1 and (b) M_2. Blue/red curves are solutions for semi-infinite/finite Area2. The red arrow indicates the position of the connecting point between the Korea Strait and the Japan Sea. Amplitudes are given as ratios to the incident wave in Area1.

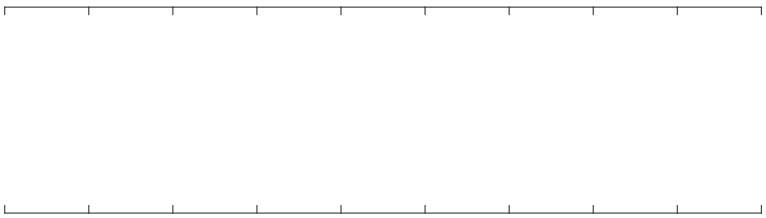

Figure 10: Phase-lag increase of the reflected wave relative to the incident wave as a function of the angular frequency at the connecting point. See the text for details.

5 Summary

In this paper, we establish a theoretical model for the KS-JS basin using the extended Taylor method. The model idealizes the study region as three connected flat rectangular areas, incorporates the effects of the Coriolis force and bottom friction in the governing equations and is forced by observed tides at the opening of the KS. The analytical solutions of the K_1 and M_2 tidal

waves are obtained using Defant's collocation approach.

The theoretical model results are consistent with the satellite altimeter and tidal gauge observations, which indicates that the model is suitable and correct. The model well reproduces the K_1 and M_2 tidal systems in the KS. In particular, the model-produced locations of the K_1 and M_2 amphidromic points are consistent with the observed ones.

The model solution provides the following insights into the tidal dynamics in the KS. (1) The tidal system in each rectangular area can be decomposed into two oppositely travelling Kelvin waves and two families of Poincaré modes, with Kelvin waves dominating the tidal system due to narrowness of the area. (2) The incident Kelvin wave from the ECS through the opening of the KS travels toward the JS and is reflected at the connecting cross-section between the KS and JS, where abrupt increases from the KS to JS in water depth and basin width occur. (3) The phase lag of the reflected wave at the connecting cross-section increases by less than 180° relative to that of the incident wave, thus enabling the formation of the amphidromic points in the KS. (4) The phase-lag increase of the reflected wave relative to the incident wave is dependent on the angular frequency of the wave and becomes smaller as the angular frequency decreases. This feature explains why the K_1 amphidromic point is located farther away from the connecting cross-section in comparison to the M_2 amphidromic point. (5) The length, width and depth of the JS is also important in determining the phase-lag increase of the reflected Kelvin wave in the KS.

Date availability. The ETOPO1 data (doi: 10.7289/V5C8276M) is from the National Geophysical Center, USA (https://www.ngdc.noaa.gov/mgg/global/). The DTU10 tidal data is from DTU Space, Danish National Space Center, Technical University of Denmark (ftp://ftp.space.dtu.dk/pub/DTU10).

Author contributions. GF conceived the study scope and the basic dynamics. DW performed calculation and prepared the draft. ZW and XC checked model results.

Competing interests. The authors declare that they have no conflict of interest.

Acknowledgments. We sincerely thank Dr. Joanne Williams for handling our manuscript and thank Dr. David Webb and the anonymous Referee for their careful reading of our manuscript and constructive comments and suggestions which are of great help in improving our work. This work was supported by the National Natural Science Foundation of China under Grant Nos. 41706031 and 41821004.

Deleted: A one-dimensional model is also given in this paper to reveal the underlying basic dynamics of tides in the KS. .

.

Appendix: Tidal wave propagation in channels with abrupt depth/width changes. .

a. Basic Equations .

We study tidal wave propagation in channels with abrupt depth/width changes. To be specific, we consider a one-dimensional problem corresponding to the model shown in Fig. 3. For simplicity, Area3 is combined into Area2, and the Coriolis force and friction are neglected, then Eqs. (10) and (11) in the Sect. 2.2 of the text can be simplified as follows: .

$u_{1,-}(x) = -a_1 \exp[ik_1(x - l_1)]$

(A1) .

$\zeta_{1,-}(x) = p_1 a_1 \exp[ik_1(x - l_1)]$

(A2) .

$u_{1,+}(x) = b_1 \exp[-ik_1(x - l_1)]$

(A3) .

$\zeta_{1,+}(x) = p_1 b_1 \exp[-ik_1(x - l_1)]$

(A4) .

$u_{2,-}(x) = -a_2 \exp[ik_2(x - l_2)]$

(A5) .

$\zeta_{2,-}(x) = p_2 a_2 \exp[ik_2(x - l_2)]$

(A6) .

$u_{2,+}(x) = b_2 \exp[-ik_2(x - l_2)]$

(A7) .

$\zeta_{2,+}(x) = p_2 b_2 \exp[-ik_2(x - l_2)]$

(A8) .

where $k_j = \sigma/c_j$ is the wave number, with $c_j = \sqrt{gh_j}$ ...

Moved up [1]: Eq. (

Deleted: A15) by p_1/h_1W_1 and obtain .

$\zeta_{1,+}(l_2) - \zeta_{1,-}(l_2) = \rho[\zeta_{2,+}(l_2) - \zeta_{2,-}(l_2)]$,

(A16) .

where .

$\rho = \frac{p_1 h_2 W_2}{p_2 h_1 W_1} = \frac{\sqrt{h_2} W_2}{\sqrt{h_1} W_1}$.

(A17) .

b. Solution for the case with semi-infinite Area2 .

Here, we first investigate a simpler case that has been previously studied by Dean and Dalrymple (1984). In this case, Area2 is assumed to be semi-infinitely long so that the wave can propagate freely in the positive *x* direction without reflection, meaning that $a_2 = 0$. Thus, the terms $\zeta_{2,-}$ in Eqs. (A6), (A14) and (A16) are all equal to zero. From Eqs. (A14) and (A16) with $\zeta_{2,-}(l_2) = 0$ we obtain . ...

References

Book, J. W., Pistek, P., Perkins, H., Thompson, K. R., Teague, W. J., Jacobs, G. A., Suk, M. S., Chang, K. I., Lee, J. C., and Choi, B. H.: Data Assimilation modeling of the barotropic tides in the Korea/Tsushima Strait. J. Oceanogr., 60, 977-993, https://doi.org/10.1007/s10872-005-0006-6, 2004.

Carbajal, N.: Two applications of Taylor's problem solution for finite rectangular semi-enclosed basins. Cont. Shelf Res., 17, 803–808, https://doi.org/10.1016/S0278-4343(96)00058-1, 1997.

Cheng, Y. C., and Andersen, O. B.: Multimission empirical ocean tide modeling for shallow waters and polar seas. J. Geophys. Res. Oceans, 116, 1130-1146, https://doi.org/10.1029/2011JC007172, 2011.

Choi, B. H., Kim, D. H., and Fang, Y.: Tides in the East Asian Seas from a fine-resolution global ocean tidal model. Mar. Technol. Soc. J., 33, 36–44, https://doi.org/10.4031/MTSJ.33.1.5, 1999.

Dean, G., and Dalrymple, R.: Water wave mechanics for engineers and scientists, World Scientific, 353 pp, 1984.

Defant, A.: Physical oceanography, Vol. II, Pergamon Press, 598 pp, 1961.

Fang, G., and Wang, J.: Tides and tidal streams in gulfs, Oceanol. Limnol. Sin., 8, 60–77, 1966. (in Chinese with English abstract).

Fang, G.: Nonlinear effects of tidal friction. Acta Oceanol. Sin., 6 (Supp1. 1), 105-122, 1987.

Fang, G., and Yang, J.: Modeling and prediction of tidal currents in the Korea Strait. Prog. Oceanogr., 21, 307–318, https://doi.org/10.1016/0079-6611(88)90010-9, 1988.

Fang, Z., Ye, A., and Fang, G.: Solutions of tidal motions in a semi-closed rectangular gulf with open boundary condition specified. Tidal Hydrodynamics, B. B. Parker, Ed., John Wiley & Sons. Inc., 153-168, 1991.

Godin, G.: Some remarks on the tidal motion in a narrow rectangular sea of constant depth. Deep-Sea Res., 12, 461-468, https://doi.org/10.1016/0011-7471(65)90400-6, 1965.

Hendershott, M. C., and Speranza, A.: Co-oscillating tides in long, narrow bays; the Taylor problem revisited. Deep-Sea Res. 18, 959-980, https://doi.org/10.1016/0011-7471(71)90002-7, 1971.

International Hydrographic Bureau: Tides, Harmonic Constants. International Hydrographic Bureau, Special Publication No. 26 and addenda, 1930.

Inoue, R. and Garrett, C.: Fourier Representation of Quadratic Friction, J. Phys. Oceanogr., 37, 593-610, https://doi.org/10.1175/JPO2999.1, 2007.

Jung, K. T., Park, C. W., Oh, I. S., and So, J. K.: An analytical model with three sub-regions for M_2 tide in the Yellow Sea and the East China Sea. Ocean Sci. J., 40, 191-200, https://doi.org/10.1007/BF03023518, 2005.

Kang, S. K., Lee, S. R., and Yum, K. D.: Tidal computation of the East China Sea, the Yellow Sea and the East Sea. Oceanography of Asian Marginal Seas, K. Takano, Ed., Elsevier, 25-48, https://doi.org/10.1016/S0422-9894(08)70084-9,

1991.

Matsumoto, K., Takanezawa, T., and Ooe, M.: Ocean tide models developed by assimilating TOPEX/POSEIDON altimeter data into hydrodynamical model: a global model and a regional model around Japan. J. Oceanogr., 56, 567-581, https://doi.org/10.1023/A:1011157212596, 2000.

Morimoto, A., Yanagi, T., and Kaneko, A.: Tidal correction of altimetric data in the Japan Sea. J. Oceanogr., 56, 31-41, https://doi.org/10.1023/A:1011158423557, 2000.

Odamaki, M.: Tides and tidal currents in the Tusima Strait. J. Oceanogr., 45, 65-82, https://doi.org/10.1007/BF02108795, 1989a.

Odamaki, M.: Co-oscillating and independent tides of the Japan Sea. J. Oceanogr. Soc. Jpn, 45, 217-232, https://doi.org/10.1007/BF02123465, 1989b.

Ogura, S.: The Tides in the Seas Adjacent to Japan. Bulletin of the Hydrographic Department, Imperial Japanese Navy, 7, 189 pp, 1933.

Pingree, R. D., and Griffiths, D. K.: The N2 tide and semidiurnal amphidromes around the British Isles. J. Mar. Biol. Assoc. U. K., 61, 617-625, https://doi.org/10.1017/S0025315400048086, 1981.

Rienecker, M. M., and Teubner, M. D.: A note on frictional effects in Taylor's problem. J. Mar. Res., 38, 183-191, 1980.

Roos, P. C., and Schuttelaars, H. M.: Influence of topography on tide propagation and amplification in semi-enclosed basins. Ocean Dyn., 61, 21-38, https://doi.org/10.1007/s10236-010-0340-0, 2011.

Roos, P. C., Velema, J. J., Hulscher, S. J. M. H. and Stolk, A.: An idealized model of tidal dynamics in the North Sea: Resonance properties and response to large-scale changes. Ocean Dyn., 61, 2019–2035, https://doi.org/10.1007/s10236-011-0456-x, 2011.

Takikawa, T., Yoon, J. H., and Cho, K. D.: Tidal Currents in the Tsushima Straits estimated from ADCP data by ferryboat. J. Oceanogr., 59, 37-47, https://doi.org/10.1023/A:1022864306103, 2003.

Taylor, G. I.: Tidal oscillations in gulfs and rectangular basins. Proc. London Math. Soc., Ser. 2, 20, 148-181, https://doi.org/10.1112/plms/s2-20.1.148, 1922.

Teague, W. J., Perkins, H. T., Jacobs, G. A., and Book, J. W.: Tide observation in the Korea-Tsushima Strait. Cont. Shelf Res., 21, 545–561, https://doi.org/10.1016/S0278-4343(00)00110-2, 2001.

Thiebaux, M. L.: Low-frequency Kelvin wave reflection coefficient. J. Phys. Oceanogr., 18, 367-372, https://doi.org/10.1175/1520-0485(1988)018<0367:LFKWRC>2.0.CO;2, 1988.

Webb, D. J.: A model of continental-shelf resonances. Deep-Sea Res., 23, 1-15, https://doi.org/10.1016/0011-7471(76)90804-4, 1976.

Wu, D., Fang, G., Cui, X., and Teng, F.: An analytical study of M_2 tidal waves in the Taiwan Strait using an extended Taylor

method. Ocean Sci., 14, 117-126, https://doi.org/10.5194/os-14-117-2018, 2018.